

**Development and Evaluation of A 3D Reconstruction
Framework for General Objects**

by

Kai Wu

Bachelor of Engineering, Beijing University of Posts and Telecommunications
2014

A THESIS SUBMITTED IN PARTIAL FULFILLMENT
OF THE REQUIREMENTS FOR THE DEGREE OF

Master of Applied Science

in

THE FACULTY OF APPLIED SCIENCE
(Department of Electrical and Computer Engineering)

The University of British Columbia
(Vancouver)

April 2017

© Kai Wu, 2017

Abstract

Advancements in state-of-the-art 3D reconstruction algorithms have sped ahead of the development of interfaces or application programming interfaces (APIs) for developers, especially to those who are not experts in computer vision.

We have designed a novel interface, specifically for 3D reconstruction techniques, which uses a description (covering the conditions of the problem) to allow a user to reconstruct the shape of an object without knowledge of 3D vision algorithms. The interface hides the details of algorithms by using a description of visual and geometric properties of the object. Our interface interprets the description and chooses from a set of algorithms those that satisfy the description. We show that this description can be interpreted to one appropriate algorithm, which can give a successful reconstruction result.

We evaluate the interface through a proof-of-concept interpreter, which interprets the description and invokes one of three underlying algorithms for reconstruction. We demonstrate the link between the description set by the user and the result returned using synthetic and real-world datasets where each object has been imaged with the appropriate setup.

Preface

The entire work presented here has been done by the author, Kai Wu, with the collaboration and supervision of Dr. Sidney Fels and Dr. Gregor Miller. A manuscript describing the core of our work and our results has been submitted to the IEEE Winter Conference on Application of Computer Vision (2018) and is under anonymous review at the moment of thesis submission.

Table of Contents

Abstract	ii
Preface	iii
Table of Contents	iv
List of Tables	viii
List of Figures	x
List of Acronyms	xv
Acknowledgments	xvi
Dedication	xvii
1 Introduction	1
1.1 Outline	3
1.1.1 Related Work	3
1.1.2 A Problem space of 3D Reconstruction	3
1.1.3 A Description of 3D Reconstruction	4
1.1.4 A Mapping of 3D Reconstruction	4
1.1.5 An Interpretation of 3D Reconstruction	4
1.2 Contributions	5
1.3 Organization	5

2	Related Work	6
2.1	Toolboxes	6
2.2	3D Reconstruction Techniques	7
2.2.1	Stereo	7
2.2.2	Structured Light	11
2.2.3	Shading	12
2.2.4	Silhouette	17
2.2.5	Limists: VH	19
3	A Problem Space of 3D Reconstruction	21
3.1	Problem space	22
3.2	Assumptions	23
3.2.1	Simplified light interaction model	23
3.2.2	Simplified reflectance model	24
3.2.3	Simplified geometric model	24
3.2.4	Simplified surface albedo	25
3.3	Four problem conditions	25
4	A Description of 3D Reconstruction	26
4.1	Model	27
4.2	Representation	27
4.2.1	Texture	27
4.2.2	Lightness	28
4.2.3	Specularity	30
4.2.4	Roughness	31
4.2.5	Perception of properties	32
4.2.6	Summary	33
4.3	Expression	34
5	A Mapping of 3D Reconstruction	36
5.1	Synthetic setup	37
5.2	Selected and baseline methods	38
5.3	Quantitative measures	38
5.4	Effective Problem Domain (EPD)	39

5.4.1	EPD: PMVS	40
5.4.2	EPD: EPS	43
5.4.3	EPD: GSL	48
5.5	Mapping Construction	51
5.5.1	Mapping: PMVS	51
5.5.2	Mapping: EPS	53
5.5.3	Mapping: GSL	53
5.6	Evaluation of Mapping	55
5.6.1	Synthetic Datasets	57
5.6.2	Conclusion	60
5.7	Summary	60
6	An Interpretation of 3D Reconstruction	64
6.1	Evaluation Methodology	65
6.1.1	Evaluation question	65
6.1.2	Criteria	65
6.1.3	Roadmap	66
6.2	Interpreter	66
6.3	Overview of Datasets	67
6.3.1	Data capture	68
6.3.2	Calibration	69
6.4	Evaluation of Interpreter	70
6.4.1	Synthetic Datasets	70
6.4.2	Real-world Datasets	72
6.5	Sensitivity analysis	73
6.6	Summary	73
7	Conclusions	75
7.1	Future directions	76
7.1.1	Geometric Model	76
7.1.2	Property Parameters	76
7.1.3	Metrics	77
7.1.4	Mapping Construction	77

7.1.5	Interpreter	77
7.2	Closure	77
	Bibliography	78
	A Supporting Materials	85
A.1	Definition of 3D Reconstruction	85
A.1.1	Basic notations	85
A.1.2	Segment and Scell	86
A.1.3	Consistency	87
A.1.4	Formal Definition	87
A.1.5	Applied Definition	88
A.2	Definition of Radiometric Terms	88
A.3	Material of real-world objects	89
A.4	Parameters of real-world objects	89
A.5	Results of real-world objects	89

List of Tables

Table 2.1	Classes of algorithms that utilize each visual/geometric cue. Note that the abbreviations will be used extensively in the thesis.	8
Table 2.2	Assumptions made by different classes of photometric stereo. . .	14
Table 4.1	Model of the 3D reconstruction problem. Properties are selected from the taxonomy in Chapter 3.	27
Table 4.2	A Model and corresponding representations of the 3D reconstruction problem.	34
Table 4.3	Expression of the reconstruction problem for the four problem conditions proposed in Section 3.	35
Table 5.1	Summary of synthetic setups.	37
Table 5.2	Summary of the selected and baseline algorithms for the interface, and the corresponding working conditions in theory. . . .	38
Table 5.3	Problem conditions for establishing the <i>effective problem domain</i> of all selected algorithms. For instance, cond. (a) considers texture and albedo while specularity and roughness are fixed. The value of both varying properties range from 0.2 to 0.8.	40
Table 5.4	The <i>effective problem domain</i> of PMVS in terms of accuracy and completeness.	43
Table 5.5	The <i>effective problem domain</i> of EPS in terms of the <i>angular error</i>	48
Table 5.6	The <i>effective problem domain</i> of GSL in terms of accuracy and completeness.	51

Table 5.7	The working problem conditions of PMVS in terms of the two metrics <i>accuracy</i> and <i>completeness</i>	53
Table 5.8	The working conditions of example-based PS in terms of the metric <i>angular error</i>	55
Table 5.9	The condition matrix of Gray-code SL in terms of the two metrics <i>accuracy</i> and <i>completeness</i>	57
Table 5.10	Property settings of the three testing objects: ‘bottle’, ‘knight’, ‘king’, which have increasing degree of concavity.	58
Table 6.1	Problem conditions and interpreted algorithm of the synthetic objects. The description matches the problem condition of corresponding object. The last column shows the algorithm selected by the interpreter.	70
Table 6.2	Problem conditions and interpreted algorithm of the real-world objects. The description matches the problem condition of corresponding object. The last column shows the algorithm selected by the interpreter.	73
Table A.1	Images of the real-world objects.	90
Table A.2	Property list for the real-world objects	92

List of Figures

Figure 1.1	The three layers of the 3D reconstruction interface.	3
Figure 2.1	Illustrations of MI-based VH. (a) shows one object (top left) and its silhouette with 2D lines traced over it to find intersections along rays in the X, Y and Z ray-set of the MI, respectively. (b) shows the MI data structure and conversion algorithm in a 2D example. Image courtesy of M. Tarini.	19
Figure 3.1	A list of properties for object classes.	23
Figure 3.2	Embed algorithms into the interface.	24
Figure 3.3	Four classes of problem conditions of interest with the proposed label.	25
Figure 4.1	The light-matter interaction. Scene radiance is linearly related to incident radiance.	29
Figure 4.2	The light-lens interaction. Image irradiance is linearly related to scene radiance.	29
Figure 4.3	The light-sensor interaction. Pixel intensity is linearly related to image irradiance assuming linear radiometric mapping.	30
Figure 4.4	(a). A red diffuse sphere; (b). a red specular sphere. The surface reflects light in a mirror-like way, showing a distorted environment. Since no diffuse reflection exists, the colour of the surface is no longer visible.	31

Figure 4.5	The UI for determining the property settings, including albedo, specular, and roughness of the surface. In this case shown above, the problem condition is: texture (0.8), albedo (0.8), specular (0.2), roughness(0.2). (a) demonstrates the effect of the property settings on a sphere, (b) on a teapot, and (c) shows the real-world object.	34
Figure 5.1	Example synthetic images. The value of each property ranges from 0.1 to 1.	37
Figure 5.2	Performance of PMVS under six pairwise conditions. For instance, (a) shows the performance under changing <i>texture</i> and <i>albedo</i> values, while the others are fixed. The property values are set based on settings in Table ??	41
Figure 5.3	(a) shows the reflection of light off a specular surface. V_1 received the diffuse component while V_2 receives the specular component. (b), (c) shows the images observed from these two views. The specular area (red circle) observed in V_2 is visible in V_1	42
Figure 5.4	(a)-(c). The albedo is set as 0.2, (d)-(f). The specularity is set as 0.2. According to energy conservation, as the specular component increases, the diffuse component decreases.	42
Figure 5.5	Performance of Example-based PS under six pairwise conditions. For instance, (a) shows the performance under changing <i>texture</i> and <i>albedo</i> values. The property values are assigned based on the settings in Table ?? (a).	44
Figure 5.6	(a)-(c). The texture is set as 0.5. The estimated normal map and recovered surface becomes consistently worse as the specular level rises, which is consistent with the quantitative results from Figure 5.5 (b).	45

Figure 5.7	According to energy conservation, as the specular component increases, the diffuse component decreases. (a)-(c): the estimated normal map and recovered height map become consistently worse as the albedo decreases; (c)-(e): the estimated normal map and recovered height map become consistently worse as the specularity increases.	46
Figure 5.8	The effect of roughness on PS. Albedo is set as 0.8, and specular is set as 0.8. (b) demonstrates that a medium level roughness would lead to worse normal estimation since it blurs the specular lobe.	47
Figure 5.9	Performance of Gray-encoded SL under six pairwise conditions. For instance, (a) shows the performance under changing <i>texture</i> and <i>albedo</i> values. The property values are assigned based on settings in Table ?? (a).	49
Figure 5.10	(a)-(c): the specular is set as 0.2, albedo has a positive effect on completeness; (d)-(e): the albedo is set as 0.2, specular has a negative effect on completeness.	50
Figure 5.11	(a)-(c): the roughness is set as 0.2, and specular has a negative effect on completeness; (d)-(e): the specular is set as 0.8, roughness has a positive effect on completeness.	50
Figure 5.12	Performance of PMVS under varied conditions of changing property values. The baseline method serves as the guidelines to determine the performance of PMVS.	52
Figure 5.13	Performance of EPS under varied conditions of changing property values. Varied statistical measures of angular error are compared to the baseline method to determine the performance of EPS.	54
Figure 5.14	Performance of GSL under varied conditions of changing property values. The baseline method serves as the guideline to determine the performance of GSL.	56

Figure 5.15	The synthetic dataset and groundtruth for the evaluation of the robustness of the mapping to concavity. Three objects with varied degrees of concavity are selected, each is configured with four properties settings listed in Table 5.10.	58
Figure 5.16	The first column shows the best algorithm chosen by the mapping. The quantitative and qualitative performance of each technique on the synthetic dataset is also shown. The red dots represent the ground truth while the black dots represent the reconstruction.	59
Figure 5.17	The first column shows the best algorithm chosen by the mapping. The quantitative and qualitative performance of each technique on the synthetic dataset is also shown. The red dots represent the ground truth while the black dot represent the reconstruction.	61
Figure 5.18	The first column shows the best algorithm chosen by the mapping. The quantitative and qualitative performance of each technique on the synthetic dataset is also shown. The green dots represent the ground truth while the black dots represent the reconstruction.	62
Figure 6.1	Two components of the Interpreter layer. The metric comparator compares the quantitative measures based on the constraints. If ‘acc-first’ is selected, the comparator favours algorithms with lower accuracy value, whereas if ‘cmplt-first’ is selected, the comparator favours algorithms with higher completeness. If ‘shape-first’ is selected, the comparator favours algorithms with lower angular error.	67
Figure 6.2	(a)-(d): Synthetic dataset, and (e)-(h) real-world dataset for evaluation.	68

Figure 6.3	The evaluation of interpreter using synthetic objects. The first column presents the description provided to the interpreter. Description i matches with the problem condition of synthetic object i , which is labeled in green rectangle. The last column is the algorithm selected by the interpreter. Since the interpreter would return a successful reconstruction given a description that matches the problem condition, the quality of reconstruction of the labeled objects indicates success/failure of the interpreter.	71
Figure 6.4	The representatives of the four classes of objects used for evaluation.	72
Figure 6.5	The evaluation of interpreter using real-world objects. The first column presents the description provided to the interpreter. Description i matches with the problem condition of synthetic object i , which is labeled in green rectangle. The last column is the algorithm selected by the interpreter. Since the interpreter would return a successful reconstruction given a description that matches the problem condition, the quality of reconstruction of the labeled objects indicates success/failure of the interpreter.	74
Figure A.1	Relation between a scell and a segment	86
Figure A.2	Illustration of light-matter interaction.	89
Figure A.3	Reconstruction results of MVS, PS, SL, and the baseline method VH.	91
Figure A.4	Reconstruction results of MVS, PS, SL, and the baseline method VH (cont'd).	92

List of Acronyms

- **3D**: 3-dimensional
- **BRDF**: Bi-directional Reflectance Distribution Function
- **CAD**: Computer Aided Design
- **DoF**: Degree of Freedom
- **EPD**: Effective Problem Domain
- **EPS**: Example-based Photometric Stereo
- **GSL**: Gray code Structured Light
- **MVS**: Multi-View Stereo
- **PMVS**: Patch-based Multi-View Stereo
- **PS**: Photometric Stereo
- **SfS**: Shape from Shading
- **SL**: Structured Light
- **VH**: Visual Hull

Acknowledgments

I want to thank my supervisor, Professor Sidney Fels, for offering me this opportunity to pursue this research direction, and provide invaluable guidance in the supervision of this thesis. I'm also deeply indebt to Dr. Gregor Miller for his mentorship and constant words of encouragement to keep me sane.

I want to thank my labmates for making it such a delight to come to work everyday. I'm thankful for all the white board discussion, coding and experimenting, and late night grinding before deadlines. Those are the memories I will cherish for the rest of my life.

Last but not least, thanks to my family for their unconditional support, especially in times of stress.

Dedication

献给我的爷爷吴国利先生

Chapter 1

Introduction

Modeling of the 3D world has been an active research topic in computer vision for decades and has a wide range of applications including 3D mapping and navigation, online shopping, 3D printing, computational photography, video games, visual effects, and cultural heritage archival. The goal of 3D modeling is to reconstruct a 3D geometric model represented by point cloud, voxel grid, depth maps, or surface mesh, from RGB or range sensors, optionally incorporating the material of the surface.

Achieving this goal is an extremely challenging task, as it involves the reverse process of image formation, which is highly likely to result in a variety of possible results and solutions. To overcome this challenge, some assumptions must be made in terms of materials, viewpoints, and lighting conditions. In turn, a solid understanding of the interaction of light with surface geometry and material is a prerequisite to fully take advantage of the existing techniques. In past decades, we have witnessed a variety of tools and approaches to 3D modeling applied successfully to an assortment of sub-domains, such as Computer Aided Design (CAD) tools [1], arm-mounted probes, active methods [2, 3, 9, 35] and passive image-based methods [15, 20, 22, 34]. Among the existing approaches, active techniques such as laser scanners [35], Structured Light (SL) systems [9], and Photometric Stereo (PS) [64], as well as passive methods such as Multi-View Stereo (MVS) [54], have been the most successful. Laser scanners and structured light techniques are seen to generate the most accurate results, but are generally complicated to set up and

calibrate, time consuming to scan, and demanding to store and process in terms of memory. Photometric Stereo is able to achieve highly detailed reconstruction comparable to that of laser scanners, but the true depth information is lost due to the use of a single viewpoint. Further, MVS requires minimal setup and can work in both controlled, small scale lab settings as well as outdoor, medium to large scale environments. However, the quality of reconstruction is generally noisier, and is susceptible to the texture and material property of the surface. All of the aforementioned techniques require an understanding of calibration, stereo correspondence, physics-based vision, and so on, which are not easy tasks to master.

Regardless of past successes and strong demands across various areas, we have not yet witnessed any substantial progress in terms of making the mentioned techniques accessible to application developers or system designers (termed *users* for the rest of the thesis), who generally have little or no computer vision expertise. We've made two key observations about computer vision algorithms: 1) few of these methods work well under all circumstances, nor do they share the same setup or inputs/outputs, making it difficult for developers to choose an optimal method for their particular application; 2) expertise knowledge is a prerequisite to fully exploit the potentials of existing vision techniques. These observations lead us to the following question which we address in this thesis: is it achievable to create an interface that can return a reliable reconstruction by one of the best possible algorithms based on the descriptions of the object or scene to be reconstructed?

The interface consists of the following three layers, see Figure 1.1: the *description layer* sits on top and acts as the medium between the user and the lower layers. It is through this that the user provides a description of the 3D reconstruction problem. The description is passed to the *interpreter* layer, which chooses appropriate algorithms given the description, and then configures each algorithm's parameters. The interpreter can also define any necessary pre or post-processing operations (such as noise removal or image scaling). The lowest layer of the three is where the *algorithms* sit.

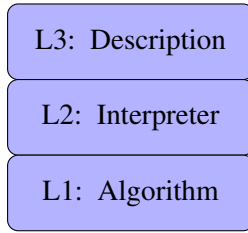


Figure 1.1: The three layers of the 3D reconstruction interface.

1.1 Outline

The problem addressed in this thesis can be described as follows: construct an interface for 3D reconstruction that can return a reliable reconstruction result by one of the best-suited algorithms, which is determined by the description of the problem condition. More specifically, a taxonomy is proposed that transforms the 3D reconstruction problem from one requiring knowledge of algorithmic details to one that is based on the correlation between the problem space and algorithms. Next, a well defined model and representations are developed to describe the problem space definitively. Lastly, mapping between the problem space and the algorithms is discovered, from which a proof-of-concept interpreter is proposed. A rigorous evaluation is then carried out to verify the robustness of the interpreter.

1.1.1 Related Work

We discuss the existing software and toolboxes for 3D reconstruction, and present the required vision background needed to fully take advantage of these toolboxes. A review of the 3D acquisition techniques is provided, organized by the visual and geometric cues used for reconstruction.

1.1.2 A Problem space of 3D Reconstruction

Existing softwares and algorithms focus on providing algorithmic solutions to problems, which we call a *algorithm-center approach*. This approach provides little insight to the problem conditions that a specific algorithm is applicable to. We proposed a *problem-centered approach* that gives a well-defined problem space, which allows further investigation of the relation between problem conditions and

algorithms. This relation can be used to choose a best possible algorithm based on described problem condition. The problem condition consists of a variety of visual and geometric properties of objects. The collective problem conditions is called *problem condition space*, or in short *problem space*.

1.1.3 A Description of 3D Reconstruction

In previous cases, the mapping from a problem space to an algorithm has been ambiguous due to the problem space that is poorly defined. Here, we set out to provide a rigorous definition of the problem space itself. First, a formal and practical definition of the 3D reconstruction problem based on set theory is proposed. Second, a model consisting of key object properties is developed. Third, the representations of the problem are proposed. Lastly, common 3D reconstruction tasks are expressed using the proposed model and representations.

1.1.4 A Mapping of 3D Reconstruction

To derive a more precise mapping from problem space to algorithm space, we need to evaluate the performance of the selected algorithms under varied properties and their combinations. We use synthetic datasets to achieve this goal. Part of the challenge in establishing a comprehensive set of experiments for such an evaluation is the large variations of shapes and material properties. To overcome this issue, we first establish the *effective problem domain* (EPD) by finding the effective properties. Then we evaluate the performance of each algorithm within the EPD, which serves as the basis of the mapping.

1.1.5 An Interpretation of 3D Reconstruction

We conduct the evaluation of the interface around two key evaluation questions: 1) can the derived mapping be extended to an object with a different shape; 2) can the proof-of-concept interpreter return a reliable result given the correct description to the problem condition. To answer these questions, we carry out two separate experiments: In Section 5.6, we use synthetic objects with the same configurations as the ones used to derive the mapping, and check if the mapping is consistent for different objects across varied problem conditions; in Section 6.4, we use synthetic

and real-world datasets to evaluate the interpreter.

1.2 Contributions

The main contribution of this thesis is the development and application of an interface for a subset of 3D reconstruction problem, which hides algorithmic details and allows users to describe conditions surrounding the problem. We focus on a subset of problem, which is defined in Chapter 3, to approach this problem in a tractable manner. This described conditions, which consists of varied visual and geometric properties, can be interpreted so that an appropriate algorithm is chosen to reconstruct a successful result. This endeavor is non-trivial for two reasons: 1) currently, most approaches can only achieve satisfactory results on a limited set of categories of objects; 2) a solid understanding of reconstruction algorithm details is a prerequisite to fully take advantage of the existing techniques, which is difficult for application developers to obtain. To some extent, our interface attempts to expand the problem space by incorporating multiple algorithms. Though it can cover a wider range of problem space than a single algorithm, it is still confined within the space covered by currently existing techniques. Thus, our evaluation is carried out within the problem space covered by the selected algorithms.

1.3 Organization

We organize this thesis as follows. Chapter 2 briefly introduces 3D reconstruction toolboxes and gives an overview of current landscape of 3D reconstruction field. In Chapter 3, we propose a simplified problem space of 3D reconstruction problems and propose four problem conditions that will be investigated in depth. In Chapter 4, we provide a formal description of problem condition of a 3D reconstruction problem. In Chapter 5, we develop the relation from problem condition to algorithms by evaluating the performance of a selection of algorithms under varied problem conditions. In Chapter 6, we use both synthetic and real-world datasets to demonstrate the interpretation of the 3D reconstruction description and the robustness of the proof-of-concept interpreter.

Chapter 2

Related Work

Section 2.1 discusses the existing toolboxes for 3D reconstruction. Section 2.2 presents a comprehensive review of the field of image-based 3D reconstruction based on varied visual/geometric cues, which include *stereo correspondence, shading, silhouette, texture distortion, and (de)focus*.

2.1 Toolboxes

There have been many attempts in developing computer vision or image processing frameworks that support rapid development of vision applications. There are multiple general vision libraries in this field including OpenCV [12], VLFeat [60], VXL [4] and multiple Matlab libraries [33, 40]. These libraries often provide tools for multiple image processing and computer vision problems, including low-vision tasks such as feature detection and matching, middle-level vision tasks such as segmentation and tracking, and high-level vision problems such as classification and recognition. All of these software frameworks and libraries provide vision components and algorithms without any context of how and when they should be applied. As a result, they often require expert vision knowledge for effective use. For example, many feature detectors/descriptors are provided by OpenCV but with no indication of under what conditions each works most effectively.

We have witnessed many successful softwares in the field of image-based reconstruction, which is a sub-field of 3D reconstruction. One of the most widely

used open source softwares is PMVS developed by Furukawa [20], which is used not only by computer vision/graphics engineers, but also production companies like Industrial Light & Magic, and Google, etc. It's often used together with Bundler, which is a Structure from Motion software that estimate camera parameters from images developed by Noah Snavely [58], and Poisson Surface Reconstruction developed by Michael Misha Kazhdan, which is a surface mesh software that estimate the triangulated surface from oriented point cloud [32]. Some other notable open source softwares include VisualSfM [65], CMP-MVS [25], MVE [19], and openMVG [43]. However, effective use of those software requires a basic understanding of the relevant domain, including feature detection, matching, camera calibration, dense correspondence search, etc.

This current situation motivates us to provide an description-based interface for non-vision users to access the state-of-the-art techniques in their own applications.

2.2 3D Reconstruction Techniques

Image-based 3D reconstruction attempts to recover the geometry and material (optional) of the object from images under different viewpoints or illuminations. The end goal here can be described as “given a set of images of an object or a scene, estimate the most likely 3D shape that explains those images, under the assumption of known materials, viewpoints, and lighting conditions”. This definition reveals that if these assumptions are violated, this becomes an ill-posed problem since multiple combinations of geometry, viewpoint and illumination can produce exactly the same images [47]. Thus this makes for an extremely challenging task.

The 3D reconstruction technique exploits a variety of visual and geometric cues to extract geometry from images: stereo correspondence, shading, contour, texture, (de)focus, etc. Please refer to Table 2.1 for an overview, where the algorithms are organized based on the cue used for reconstruction.

2.2.1 Stereo

Stereo correspondence is one of the most widely used visual cues in 3D vision. Passive methods, including stereoscopy, trinocular stereo, and MVS, identify correspondences across different views, and estimate the 3D point by triangulation.

Cue	Algorithm
Stereo correspondence	Stereoscopy Trinocular Stereo Multi-view Stereo (MVS) Laser scanning Structured light (SL)
Shading	Shape from Shading (SfS) Photometric Stereo (PS)
Contour	Shape from Silhouette (SfS)
Texture	Shape from Texture
(De)focus	Shape from (De)focus

Table 2.1: Classes of algorithms that utilize each visual/geometric cue. Note that the abbreviations will be used extensively in the thesis.

However these passive approaches suffer from uniform or periodic surfaces. Active techniques attempt to overcome the correspondence problem by replacing one of the cameras with a controllable illumination source, e.g., single-point laser, slit laser scanner, temporal or spatially modulated Structured Light (SL), etc. Here we refer readers to the survey article by Blais for recent developments of active methods. We classify the MVS algorithms based on the taxonomy proposed in [54], which divides the field into four classes based on reconstruction method, and categorize the SL algorithms by projection patterns.

Multi-View Stereo

Volumetric stereo The first class of MVS algorithms computes the cost function in a 3D volume, then extracts a surface from this volume. One successful example is voxel colouring, which traverses a discretized 3D space in depth-order to identify voxels that have a unique colouring, constant across all possible interpretations of the scene [53]. Another thread of work formulates the problem in the Markov Random Field (MRF) framework and extracts the optimal surface by Graph-Cut algorithms [49, 61, 62].

Surface Evolution The second class of MVS algorithms works by iteratively evolving a volume or surface to minimize a cost function. This includes meth-

ods based on voxels, level set, and surface meshes. The Space Carving technique achieves a least-commitment shape [41] by iteratively removing inconsistent voxels from the scene [34]. Level-set techniques cast the problem as a variational one, and use a set of PDE’s as cost functions, which are deformed from an initial set of surfaces towards the detected objects [15]. Other approaches use a deformable model and represent the scene as surface meshes that moves as a function of internal and external forces [14]. Hiep et al. presented a visibility-based method that transforms a dense point cloud into a surface mesh, which is fed into a mesh-based variational refinement that captures small details, smartly handling photo-consistency, regularization and adaptive resolution.

Region Growing The third class of MVS algorithms starts with a sparse set of scene points, propagates these points to spatial neighbours, and refine the cost function with respect to position and orientation of the points. Otto and Chau proposed one of the first work on region growing stereo search. The essence of this algorithm is as follows: start with an approximate match between a point in one image and a point in another, use an adaptive least-squares correlation algorithm to produce a more accurate match, and use this to predict approximate matches for points in the neighbourhood of the first match. A two-view quasi-dense approach first sorts the list of point correspondences into a list of seed points by correlation score. At each step of the propagation, a ‘best’ seed point is chosen. Then in the immediate spatial neighborhood of this seed point, new potential matches are checked and the best points are added to the current list of seed points [36, 37]. This “best-first” strategy guarantees convergence by choosing only new matches that have not yet been selected. Further, a patch based approach is proposed that undergoes multiple iterations of matching, propagation, and filtering [20]. A stereoscopic approach called PatchMatch Stereo, which is inspired by an approximate nearest neighbour matching algorithm called PatchMatch [6]. This method starts by randomly assigning an oriented plane to each pixel in two views. Next, each pixel is taken through three iterations of propagations and refinement. The plane is propagated to spatial neighbours, the corresponding pixel from another view, and across time. It can achieve sub-pixel accuracy, but is computationally heavy and challenging for parallelism. There has been some efforts to extend PatchMatch Stereo to multi-view scenarios [21, 59, 67] and to a proposal of new propagation schemes to increase

the computational efficiency [21].

Depthmap Merging The fourth class of MVS algorithms computes a per-view depthmap. By treating a depthmap as a 2D array of 3D points, multiple depthmaps can be considered as a merged 3D point cloud. A winner-takes-all approach uses a set of discretized depth values and picks the value with the highest photo-consistency score for each pixel independently. Uniform depth sampling may suffice for simple and compact objects. However, for complex and large scenes, a proper sampling scheme is crucial to achieve high speed and quality. More sophisticated cost function are derived to account for occlusion or non-Lambertian effects which may add noise to the photo-consistency score [22, 62]. In the case of severe occlusion, spatial consistency can be enforced under the assumption that neighbouring pixels have similar depth values. This can be formulated under the Markov Random Field (MRF) framework, where the problem becomes minimizing the sum of a unary $\Phi(\cdot)$ and pairwise term $\Psi(\cdot, \cdot)$. The unary term reflects the photo-consistency score of assigning a depth value d_p from a depth set to the pixel p , whereas the pairwise term enforces the spatial regularization, and assigns the cost of setting depth label k_p, k_q to a pair of neighbouring pixels p and q , respectively.

$$E(\{k_p\}) = \sum_p \Phi(k_p) + \sum_{(p,q) \in \mathcal{N}} \Psi(k_p, k_q)$$

Limits: MVS

Texture Multi-view Stereo algorithms take advantage of textural information to establish point correspondences across different views. Thus homogeneous surfaces pose great challenges to MVS algorithms. However, some MVS algorithms tested on a textureless object “Dino” in the Middlebury MVS benchmark [54] give successful reconstruction results. This demonstrates that MVS algorithms are able to exploit very weak and intricate image textures, most of which come from shading and/or shadowing effects. However, these texture are so weak that images need to have very high quality.

Reflectance Most MVS algorithms require that the object surface with similar or same appearances from different perspectives, and hence, most of the algorithms assume Lambertian reflectance. While pure Lambertian surfaces are rare in reality,

it is empirically verified that MVS algorithms perform reasonably well on non-Lambertian surfaces. As long as the cameras can capture the diffuse reflectance component, and then the photo-consistency function is able to identify and ignore images whose non-diffuse effects (e.g., specular highlights) are strong, then utilize the diffuse component in the remaining images. Further, there are some attempts to overcome this limitation, a pure passive methods was proposed that directly model and analyze non-Lambertian effects for MVS algorithms [30, 31].

2.2.2 Structured Light

Structured light is considered one of the most accurate reconstruction techniques. It is based on projecting a temporally or spatially modulated pattern onto a surface and viewing the illuminated surface from one or more points of view. The correspondence is easily detected from the projected and imaged pattern, which is triangulated to obtain the a 3D point. Each pixel in the pattern is assigned a unique codeword, and the codeword is encoded by using grey level, colour or geometric representations. Structured light is classified based on the following coding strategy: temporal, spatial and direct codification [50]. Temporal techniques generate the codeword by projecting a sequence of patterns. Spatial codification represents each codeword in a unique pattern. Direct codification techniques define a codeword for every pixel, which is equal to its grey level or colour.

Temporal encoding For temporally encoded SL, a sequence of patterns is successively projected onto the surface, the codeword for a given pixel is formed by the sequence of illumination values for that pixel across the projected patterns. This kind of pattern can achieve high accuracy due to two factors: 1) the codeword basis is small (e.g., two for binary pattern), therefore, each bit is easily distinguishable; 2) a coarse-to-fine strategy is used, and the position of the pixel becomes more precise as the patterns are successively projected. We further classify these techniques as follows: 1) binary codeword; 2) n -ary codeword; 3) gray code combined with phase shifting; 4) hybrid techniques.

Spatial encoding This technique concentrates all coding into a unique pattern. The codeword that labels a certain pixel is obtained from the neighbourhood of pixels around it. Normally, the visual features gathered in a neighbourhood are the

intensity or colour of the pixels or groups of pixels around it.

Direct encoding There are methods to directly represent the codeword in each pixel. To achieve this, we need to use either a large range of colour values or introduce periodicity. However, this kind of pattern is highly sensitive to noise because the “distance” between codewords is nearly zero. Moreover, the perceived colour depends not only on the projected colour, but also the intrinsic colour of the surface. Therefore, reference images must be taken. This kind of coding can be classified as: 1). codification based on grey levels; 2). codification based on colour.

Limits: SL

Brightness Active methods such as SL utilize reflected light to establish correspondences across different views. Regardless of which projection pattern is used, the most critical component of any SL system is the decoding process, which retrieves per-pixel codeword from the imaged projection pattern. Thus, the surface albedo needs to be strong enough so that sufficient amount of reflected light can reach the camera sensor.

Reflectance Traditional Structured Light techniques cannot deal with highly specular surfaces since the specular area will exhibit strong reflection regardless of the magnitude of the light source, which will cause errors in the decoding process.

Concavity Active methods that assumes a **local interaction model** such as most SL algorithms can work more reliably on surfaces without casting shadow and interreflection. Thus surfaces with concavities pose a great challenge for this type of techniques since the intensity can be affected by other surface patches.

2.2.3 Shading

Shading variations can reveal the surface normal orientation, which can be further integrated into a 2.5D height map. Shading variation depends on the shape (surface normal orientation), reflectance (material), and lighting (illumination). Thus an ill-posed problem arises because different shapes illuminated under different light conditions may produce the same image. This leads to a novel technique called Photometric Stereo in which surface orientation is determined from two or more images. The idea of Photometric Stereo is to vary the direction of the incident

illumination between successive views while holding the viewing direction constant. This provides enough information to determine surface orientation at each pixel [63]. This technique can produce a surface normal map with the same resolution of the input image, i.e., to produce the pixel-wise surface normal map. Since the coefficients of the normal map are continuous, the integrated height map can reach an accuracy that cannot be achieved by any triangulation methods. Therefore, the Photometric Stereo technique is more desirable if the intrinsic geometric details are of great importance.

Shape from Shading

The problem of recovering the shape of a surface from the intensity variation is first proposed by Horn [28]. It assumes that the surface under consideration is of a uniform albedo and reflectance, and that the direction of the single distant light source is either known or can be calibrated by the use of a reference object. Thus the intensity $I(x, y)$ becomes purely a function of the local surface orientation. The information of reflectance, illumination, and viewing geometry can be combined into a single function called reflectance map $R(p, q)$, that relates surface orientation directly to image intensities

$$\begin{aligned} I(x, y) &= R(p(x, y), q(x, y)) \\ I(x, y) &= \rho(\vec{n}, \vec{l}) \vec{n}^\top \vec{l} \quad (\text{Lambertian model}) \end{aligned}$$

where $(p, q) = (z_x, z_y)$ are surface gradients. Unfortunately, measurements of the brightness at a single pixel only provide one constraint, whereas surface orientation requires two. Thus, additional constraints such as smoothness or integrability are required to estimate (p, q) .

Limits: SfS

Texture: **textureless** Typical SfS algorithms assume surfaces with uniform and known albedo, i.e., textureless surfaces.

Brightness Active methods such as SfS utilize reflected light to estimate surface depth or orientation information. In this case, the intensity variation is used

to estimate surface normal, thus the surface should have sufficiently high albedo, otherwise, the intensity variation would be hard to detect.

Reflectance Though other reflectance models are feasible, typical SfS algorithms assume Lambertian reflectance model. The reason is that surface lightness is directly related to surface orientation and reflectance model once the light source and viewing direction are fixed. This is generally an ill-posed problem even with Lambertian model since there is only one intensity value per pixel to solve for surface orientation, which has two DoF. However, even in the simplest case, the survey by Zhang [66] demonstrate that SfS algorithms generally perform poorly, and none performs well in all cases.

Concavity Typical SfS algorithms can not deal with effects caused by global light transport, such as cast shadow, inter-reflection, and so on. The surface lightness would be corrupted by light transported from other surface facets. Thus, objects exhibit any form of concavity will pose great challenge to SfS algorithms.

Photometric Stereo

Category	Camera	Light source	Reflectance
Original PS	Orthographic	Directional, known intensity and direction	Lambertian
Generalized lighting PS	Orthographic	unknown intensity and direction, ambient	Lambertian
Generalized reflectance PS	Orthographic	Distant, known intensity and direction	Non-Lambertian

Table 2.2: Assumptions made by different classes of photometric stereo.

Original Photometric Stereo This method, first proposed by Woodham [64], utilized multiple light sources from different directions to overcome the ambiguity of Shape from Shading. Assuming there are P pixels per image, and Q illumination

directions, the intensity of the i th pixel under j th illumination would be

$$\begin{aligned} I_{i,j} &= \rho_i \vec{n}_i^\top \vec{l}_j \\ \Rightarrow \mathbf{I} &= \mathbf{N}^\top \mathbf{L} \end{aligned}$$

where

- $\mathbf{I} \in \mathbb{R}^{P \times Q}$ stores the pixel intensity from all images. Each column contains pixels from each image while each rows contains intensity of each pixel under all illumination conditions
- $\mathbf{N} \in \mathbb{R}^{P \times 3}$ encodes the albedo-scaled surface normal for each pixel, i.e., $N_{i,:} = \rho_i \vec{n}_i^\top$
- $\mathbf{L} \in \mathbb{R}^{3 \times Q}$ encodes the light source directions, i.e., $L_{:,j} = \vec{l}_j$

This surface reflectance, i.e., spatially varying albedo, and the normal can be estimated by

$$\begin{aligned} N &= \mathbf{I} \mathbf{L}^+ \\ \rho_i &= \|N_{i,:}\| \\ n_i &= \frac{N_{i,:}^\top}{\|N_{i,:}\|} \end{aligned}$$

The key problem is how to generalize the assumptions of photometric stereo. For the camera assumption, orthographic projection can be achieved by using a lens with long focus and placing the objects far from the camera. The nonlinear response can be solved by performing radiometric calibration. The shadow and other global light transportation are a few of the sources of errors, where some approaches consider them as outliers and remove them before normal estimation. The reflectance and lighting assumptions, however, are the most complicated since the reflectance properties depends on material property and microscopic structure. Further, lighting can have either an arbitrary or fixed position, orientation, and intensity. Therefore, research on Photometric Stereo are generally on two directions: 1). generalization of reflectance; 2). generalization of lighting conditions.

Generalization of Lighting It is possible to estimate the surface orientation without knowing light directions, a case also known as *uncalibrated Photometric Stereo*, see Table 2.2. Most uncalibrated techniques assume Lambertian techniques and are based on factorization technique proposed in [24]. Recall the Irradiance Equation:

$$I = N^\top L$$

However, an infinite number of candidates \hat{N} and \hat{L} make the above equality met. In fact, any invertible 3×3 matrix G defines a candidate pair $\hat{N} = N \cdot G, \hat{L} = G^{-1}L$. Thus the normal N and light source direction L can only be recovered up to a linear transformation.

Other generalized lighting conditions are any situations other than the ideal case of using a single distant point light source in a dark room, such as natural ambient light, multiple point light sources with/without ambient lighting, etc. To make the problem more tractable, the reflectance model should no longer be a general one, as this involves too many degrees of freedom that results in many different shapes with incorrectly estimated general reflectance and incorrectly estimated general lighting.

Generalization of Reflectance This class of techniques relax the assumption of Lambertian reflectance.

Outlier rejection The fact that the reflectance of non-Lambertian surfaces can be approximated by the sum of a diffuse and a specular lobe has been exploited extensively. The specular pixels are considered as outliers in [13] and [7]. The assumption that the color of the specular lobe differs from that of the diffuse lobe allows the separation of the specular and diffuse components [39, 51, 52].

Reference object A separate approach uses a reference object that has the same material as the target object. This is proposed in [57] and later revisited in [26]. It can deal with arbitrary BRDFs as long as the reference and target object has the same material. Multiple reference objects are needed for spatially-varying BRDFs as the BRDF at each point on the target object is a linear combination of the basis BRDFs defined by the set of reference objects.

Parametric reflectance model More sophisticated BRDF models can replace the reference objects. An isotropic Ward model is used as basis BRDF, and the

surface orientation and parameters of the reflectance models are estimated iteratively [23].

Invariants of BRDF While parametric reflectance models are very good at reducing the complexity of BRDFs, they are usually only valid for a limited class of materials. An alternative is to exploit the invariants of BRDFs, typically including energy conservation, non-negativity, Helmholtz reciprocity, isotropy, etc [5, 68].

Limits: PS

Texture Though SfS algorithms require uniform and known albedo, typical PS algorithms can be used easily on surfaces with spatially varying albedo. For instance, the albedo-scaled normal can be estimated, then the albedo is retrieved as the magnitude of the scaled normal [64].

Brightness Active methods such as PS utilize reflected light to estimate surface depth or orientation information. In this case, PS algorithms work more reliably on surfaces with sufficiently strong albedo. This is because the algorithm exploits the intensity variation as a visual cue, which is more challenging to detect on surfaces with low intensity values.

Reflectance The Lambertian PS algorithms can be divided into two groups: calibrated, and uncalibrated method. The original PS proposed by Woodham [64] can be considered as calibrated Lambertian PS. Later, more uncalibrated Lambertian PS algorithms have been proposed to avoid this tedious process.

Convexity Active methods that assumes a **local interaction model**, such as most PS algorithms, can work more reliably on surfaces without casting shadow and inter-reflection. Thus surfaces with concavities pose a great challenge for this type of techniques since the indensity can be affected by other surface patches.

2.2.4 Silhouette

In some cases, it's an easy task to perform a foreground segmentation of the object of interest, which leads to a class of techniques that reconstructs a 3D volumetric model from the intersection of the binary silhouettes projected into 3D. The resulting model is called a *visual hull*.

The basic idea of shape from silhouette algorithms is that the object lies in-

side the intersection of all visual cones back-projected from silhouettes. Suppose there are multiple views V of the target object. From each viewpoint $v \in V$, the silhouette s_v can be extracted, which is the region including the object's interior pixels and delimited by the line(s) separating the object from the background. The silhouette s_v are generally non-convex and can represent holes due to the geometry of the object. A cone-like volume $cone_v$ called (truncated) extended silhouette is generated by all the rays starting at the center of projection and passing through all the points of the silhouette. The target object is definitely internal to $cone_v$, and this is true for every view $v' \in V$; it follows that the object is contained inside the volume $c_V = \cap_{v \in V} c_v$. As the size of the V goes to infinity, and all possible views are included, c_V converges to a shape known as the *visual hull* vh of the target object.

[computational complexity] intersection of many volumes can be slow. Simple polyhedron-polyhedron intersection algorithms are inefficient. To improve performance, most methods 1) quantize volumes, 2) perform intersection computation in 2D instead of 3D.

Voxel based methods First the object space is split up into a 3D grid of voxels; each voxel is intersected with each silhouette volume; only voxels that lie inside all silhouette volumes remain part of the final shape.

Marching intersections based methods The marching intersection (MI) structure consists of 3 orthogonal sets of rays, parallel to the X , Y , and Z axis, which are arranged in 2D regular arrays, called the $X-rayset$, $Y-rayset$, $Z-rayset$ respectively. Each ray in each rayset is projected to the image plane to find the intersections with the silhouette. These intersections are un-projected to compute the 3D intersection between the ray and the extended silhouette on this ray. This process is repeated for each silhouette, and the un-projected intersections on the same ray are merged by the boolean AND operation.

Once the MI data structure representing the intersection of all extended silhouettes, a triangular mesh is extracted from it. This is done by the MI technique proposed in [48] which traverses the “virtual cells” implicitly defined by the MI, builds a proper marching cube (MC) entry for them that in turn is used to index a MC’s lookup table.

Exact polyhedral methods The silhouette is converted into a set of convex or non-convex 2D polygons with holes allowed. The resulting visual hull with

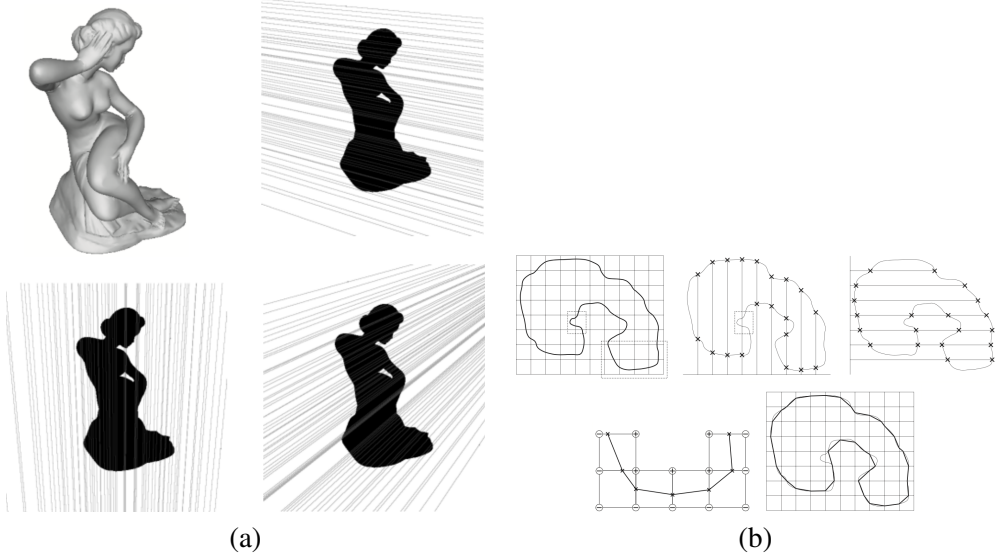


Figure 2.1: Illustrations of MI-based VH. (a) shows one object (top left) and its silhouette with 2D lines traced over it to find intersections along rays in the X, Y and Z ray-set of the MI, respectively. (b) shows the MI data structure and conversion algorithm in a 2D example. Image courtesy of M. Tarini.

respect to those polygonal silhouettes is a polyhedron. The faces of this polyhedron lie on the faces of the original cones. The faces of the original cones are defined by the center of projections and the edges in the input silhouettes. The idea of this method is: for each input silhouette s_i we compute the face of the cone. Then we intersect this face with cones of all other input silhouettes, i.e., a polygon-polyhedron intersection. The result of these intersections is a set of polygons that define the surface of the visual hull.

All of the cues above are most widely used ones, and achieved decent results. These following two cues haven't resulted in as much success. Therefore, we only discuss the general idea rather than the technical details.

2.2.5 Limists: VH

Visual Hull algorithms don't rely on material properties as long as the foreground of the image can be reliably segmented, thus is applicable for objects with arbitrary

visual properties. However, it fails to carve the concavities on the object surface, thus is unsuitable to concave objects.

Chapter 3

A Problem Space of 3D Reconstruction

Existing 3D softwares and algorithms focus solely on the algorithm-side of the problem. This provides the following hurdles: 1) they are algorithm centric, giving little to none insight to the conditions that allow a specific algorithm to work well, thus requires vision knowledge to fully take advantage of these algorithms; 2). they are unsuitable to tackle objects wide range of properties, as it is well known that such algorithms only target limited categories of objects, and are highly likely to fail when targeting a diverse set of object categories. Thus it is crucial to understand the conditions a specific algorithm performs well when designing an application for reconstruction. Under the *algorithm-centered approach* approach, this knowledge is largely empirical, with each algorithm mapped roughly to a sub-volume in the problem space that is poorly defined. To overcome these limitations, we take a more *problem-centered approach*. This approach transforms the 3D reconstruction problem from one requiring knowledge and expertise of specific algorithms in terms of *how* to use them, to one requiring knowledge of problem conditions, which can be perceptually estimated or measurable.

First, we need to have a better understanding of the problem space. In this thesis, what we mean problem space is the volume of reflectance and shape variations that objects occupy. We first describe the visual and geometric properties that constitute this problem space, then we provide further discussions regarding addi-

tional assumptions and underlying rationales to further narrow the problem space, and propose the four main problem conditions that we are interested in investigating in this thesis.

3.1 Problem space

We first give an overview of problem space, which consists of visual and geometric properties of real-world objects, as shown in Figure 3.1. These properties can be conceptualized as dimensions/axes of the 3D reconstruction problem space. This approach allows us to think of algorithms pointing to volumes within an n -dimensional problem space. Existing algorithms can be incorporated into the interface by evaluating the algorithmic performance within the problem space, as shown in Figure 3.2. However, by no means are the presented problem space complete. There are many other properties not included that are commonly seen in the real world. For instance, properties such as metalness, emission, occlusion, discontinuity, among others, are not considered. However, the listed set of properties are broad enough to encompass a wide range of real-world objects. To help easy identification of a specific problem condition, we propose the following labels to differentiate object classes.

Labels of Properties

- **Translucency:** **O:** opaque, **Tl:** translucent, **Tp:** transparent.
- **Texture:** **T:** textured, **Tr:** repeated textured, **Tl:** textureless.
- **Lightness:** **B:** bright, **D:** dark.
- **Reflection:** **D:** diffuse model, **S:** specular model, **M:** mixture of diffuse and specular, **Ss:** subsurface scattering, **Rf:** refraction
- **Roughness:** **S:** smooth, **R:** rough
- **Concavity:** **Cx:** convex, **Cv:** concave

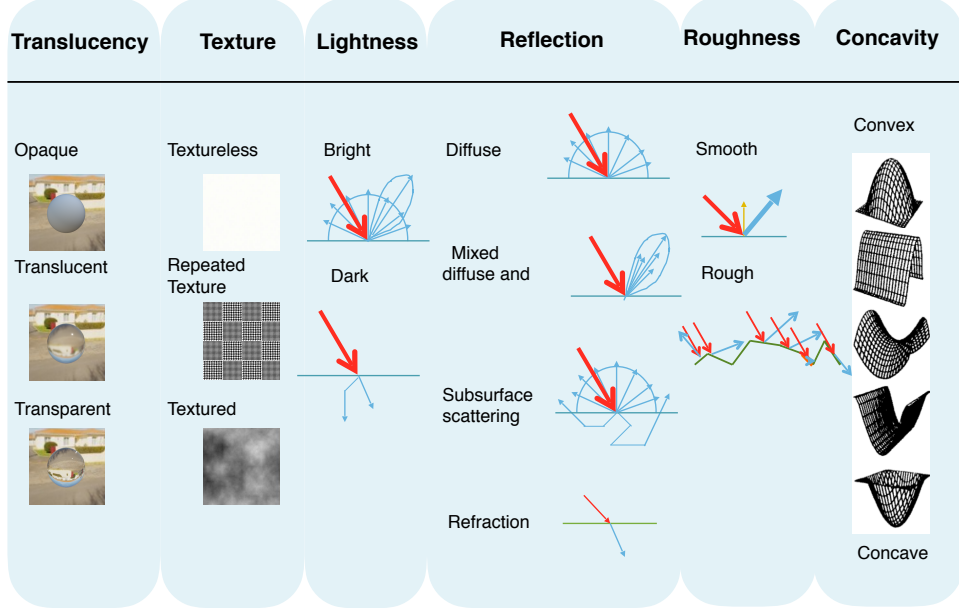


Figure 3.1: A list of properties for object classes.

3.2 Assumptions

To limit the scope of this work, we make the following assumptions:

3.2.1 Simplified light interaction model

We assume **local interaction model**, i.e., global light transport such as transmission, refraction, cast shadow, inter-reflection, metallic are not considered. The rationale behind our choice is that most techniques that have been developed over the past few decades mainly tackle object with an opaque, diffuse or mixed surface. For specular, refractive, and translucent or transparent objects, only very specialized algorithms are applicable for reconstruction [29]. This is a widely used and accepted model in varied areas of computer vision, including shape from stereo, shading, and so on. As more algorithms become available to tackle these types of objects, they can be embedded to the interface using the same approach will be discussed in Chapter 5, as shown in Figure 3.2.

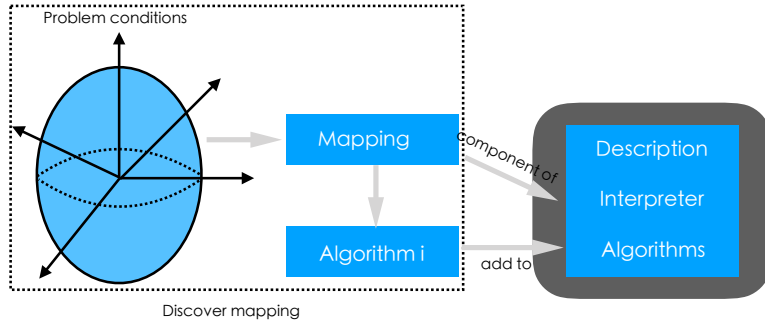


Figure 3.2: Embed algorithms into the interface.

3.2.2 Simplified reflectance model

Since the majority of reconstruction techniques rely on observing light reflected off a surface, surfaces exhibit significant effect of global light transport present a huge challenge to the reconstruction problem. Surface exhibits global light transport, including *specular*, *transmission*, *sub-surface scattering*, *inter-reflection*, *self-shadow*, and etc would break the assumptions made by most generic 3D reconstruction algorithms. Thus the global light transport are ignored, and the reflection properties of consideration are *albedo*, i.e., the ratio of reflected light w.r.t the received light, and *specularity*, i.e., the amount of specular reflection. A more comprehensive model should be constructed based on our work to incorporate more complex phenomena to be more comprehensive.

3.2.3 Simplified geometric model

It's a challenging task to model geometry using mathematical descriptions. For geometric primitives such as cube, sphere, or cone, etc, it's possible to describe the shape using concise descriptions. However, the task becomes prohibitive when it comes to shapes with varied characteristics. Furthermore it becomes more ambiguous when natural language is employed. Thus we only consider the microscopic roughness of the surface, which has a direct relation with the reflection. Other prominent geometric properties such as *concavity*, which affects self-shadow, inter-reflection, *depth-discontinuity*, which affects the depth estimation, are ignored.

3.2.4 Simplified surface albedo

Existing 3D vision techniques requires distinct cues for reconstruction, be it texture, intensity variation, focus change, and so on. This information will become much noisier and less effective on dark surfaces. Surfaces with low albedo will effectively eliminate some possible candidate algorithms including most active techniques. This works fine since only one algorithm is required to be returned by the interface. However, as an demonstrative purpose, it causes speculations as whether the lack of is due to the interface or the challenging nature of the dark surface. To better demonstrate the effectiveness of the interface, we decide to focus on bright surfaces. By making this assumption, we can avoid eliminate multiple algorithms in the first place, and see if the interpreter can pick the right one based on user's description.

3.3 Four problem conditions

Four classes of problem conditions are being investigated in depth, as shown in Figure 3.3. They are selected based on the assumptions, availability of reliable techniques and the diversity of corresponding real-world objects.

Condition	Texture	Lightness	Reflection	Roughness	Label				
	Textureless (Tl) 	Textured (T) 	Dark (D) 	Bright (B) 	Diffuse (D) 	Mixed (M) 	Smooth (S) 	Rough (R) 	
1	Yes		Yes	Yes	Yes	Tl-B-D-R			
2	Yes		Yes	Yes	Yes	Tl-B-M-S			
3		Yes	Yes	Yes	Yes	T-B-D-R			
4	Yes	Yes	Yes	Yes	Yes	T-B-M-S			

Figure 3.3: Four classes of problem conditions of interest with the proposed label.

Chapter 4

A Description of 3D Reconstruction

In Chapter 3, we introduce a taxonomy of 3D reconstruction which categorizes algorithms based on the problem space that they can reliably work under, i.e., a mapping from problem space to algorithm space. However, without a formal description, i.e., a model and representations, this mapping would be largely empirical. Expressing the conditions within which an algorithm works well without a formal definition of the problem space prevents formulating a well defined problem.

In this chapter, we attempt to provide a description of the 3D reconstruction problem which allows for a well defined specification of the conditions surrounding the problem. This description abstracts away from the functional specification of *how* to estimate a reconstruction. We first propose a formal definition of the 3D reconstruction problem in Section A.1. Next, section 4.1 proposes a model to 3D reconstruction by selecting various key *aspects* of the problem space that are crucial for describing the appearance of the object. Section 4.2 outlines concrete representations of the proposed model. Section 4.3 provides examples of expressing common 3D reconstruction problems using the proposed model and representations. These following four layers represent the description of our accessible 3D reconstruction framework: Definition, Representation, Model, and Expression.

4.1 Model

Models and representations are fundamental for vision problem solving. Models select characteristic properties of an object, and representation describes the model selected object properties to facilitate a solution of a class of problem. A model facilitates the representation of aspects in reality that are useful in a particular problem domain [11]. For instance, surface orientation is one component of the surface geometry model, and the corresponding representation can be surface normal or curvature. Another example is colour, which is a component of a material model, and where RGB space is the corresponding representation of the colour.

We select the subset of properties used for object taxonomy in Chapter ?? as the main components of our model. The model consisting of these key properties is shown in Table 4.1.

Model	Texture
	Lightness
	Reflectance
	Roughness
	Concavity

Table 4.1: Model of the 3D reconstruction problem. Properties are selected from the taxonomy in Chapter 3.

4.2 Representation

Based on the proposed definition and model of the 3D reconstruction problem, we need to further define our representations so that the 3D reconstruction problem can be expressed using our proposed model. We need to turn our attention to how to represent the properties used in the proposed model.

4.2.1 Texture

Texture is one of the most important cues for many computer vision algorithms. It is generally divided into two categories, namely *tactile* and *visual* textures. Tactile textures refer to the immediate tangible feel of a surface, whereas visual textures refer to the visual impression that textures produce to the human observer, which

are related to local spatial variations of simple stimuli like colour, orientation and intensity in an image. Here we focus only on visual textures, as they are more widely used in the stereo vision research. The term ‘texture’ hereafter refers exclusively to ‘visual texture’ unless mentioned otherwise.

Although texture is an important component in computer vision, there is no precise definition for the notion of texture itself. The main reason for this is that natural textures often exhibit separate yet contradicting properties, such as regularity versus randomness, or uniformity versus distortion, which can hardly be described in a unified manner.

There are various properties that make texture distinguishable: scale/size/granularity, orientation, homogeneity, randomness, etc. However, due to the diverse and complexe nature of textures, it is a challenging task to generate a synthetic texture solely from these semantic properties, or the other way around, derive parameters from a given texture. The stereo vision community often takes a simplified approach, classifying textures into two categories, regular and stochastic, by degree of randomness. A regular texture is formed by regular tiling of easily identifiable elements (texels) organized into strong periodic patterns. A stochastic texture exhibits less noticeable elements and displays rather random patterns. Most of the real world textures are mixtures of these two categories. In this thesis, we adopt this simplification and consider *texture randomness*, which is the amount of distortion in the texture. Thus, a uniform texture has no/low *texture randomness* whereas a highly textured surface has high *texture randomness*.

4.2.2 Lightness

When light strikes a surface, it may be reflected, transmitted, absorbed, or scattered; usually, a combination of these effects occurs. The intensity/colour information received by a sensor is thus determined, among other factors, by the amount of light available after these interactions. Here, we consider intensity as caused solely by reflection, since this is one of the most common phenomena experienced and is the easiest to analyze. Generally, we assume that all effects are local, thus global effects such as inter-reflection and transmission, among others, are omitted. This is called a **local interaction model**.

In order to understand the contributing factors of pixel intensity/colour, we need an in-depth understanding of reflection, i.e., how light is reflected off of a surface patch, and the relation between material and intensity values. The radiometric formation of an image consists of three separate processes, *light-matter interaction*, *light-lens interaction*, and *light-sensor interaction*.

Light-matter interaction

The relation between the incoming illumination and reflected light is modelled using the *bidirectional reflectance distribution function* (BRDF). The BRDF is defined as:

Definition (BRDF) the ratio of the scene radiance $\mathbf{L}_r(\theta_r, \phi_r)$ to the irradiance $E_i(\theta_i, \phi_i)$, i.e., $f(\theta_i, \phi_i, \theta_r, \phi_r) = \frac{E_{surface}(\theta_i, \phi_i)}{L_{surface}(\theta_r, \phi_r)}$.



Figure 4.1: The light-matter interaction. Scene radiance is linearly related to incident radiance.

For Lambertian model, BRDF can be simplified as *Diffuse albedo* or surface albedo, which is the proportion of incident light that is reflected by the surface.

Light lens interaction

A common assumption made in vision community is that radiance is constant as it propagates along a ray. Therefore, the scene radiance is the same as the radiance passing through the lens, which is the same as the radiance received by the sensor. Since image irradiance is the radiance accumulated on a unit surface, it follows that image irradiance is proportional to the scene radiance. Thus, the relation between *scene radiance* and *image irradiance* is linear.

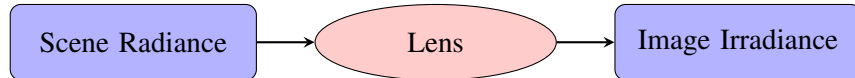


Figure 4.2: The light-lens interaction. Image irradiance is linearly related to scene radiance.

Light sensor interaction

The camera response function relating image irradiance at the image plane to measured pixel intensity values is a non-linear mapping. A linear relation can be retrieved by radiometric calibration.



Figure 4.3: The light-sensor interaction. Pixel intensity is linearly related to image irradiance assuming linear radiometric mapping.

In conclusion, as long as the *light-sensor interaction* is considered as a linear mapping (as most vision algorithms do) or calibrated in a pre-processing step, the pixel intensity value is linearly related to surface reflectance, which is characterized by BRDF. There are 4 DoF in spatially-invariant BRDF, and for the simplified case - Lambertian reflectance, the BRDF is degenerated to *diffuse albedo*, which is the representation we adopt for lightness.

4.2.3 Specularity

Specular surfaces reflect light in nearly a single direction when microscopic surface irregularities are small compared to light wavelength, and no subsurface scattering is present [44]. Unlike diffuse reflections, where we experience the lightness and colour of an object, specular reflections carry information about the structure, intensity, and spectral content of the illumination field. In other words, specular reflection is simply an image of the environment, or the illumination field, distorted by the geometry of the reflecting surface. For instance, the specular sphere in Figure 4.4 shows a distorted image of the environment instead of the underlying surface colour. A purely specular surface is a mirror, which is rare in nature. Most natural materials exhibit a mixture of specular and diffuse reflections. A commonly used model treats mixed reflectance as a weighted combination of diffuse and specular component. Thus the ratio of incident light that is specularly reflected is considered as the representation of specularity, with 0 being completely diffuse, and 1 being completely specular (mirror like).

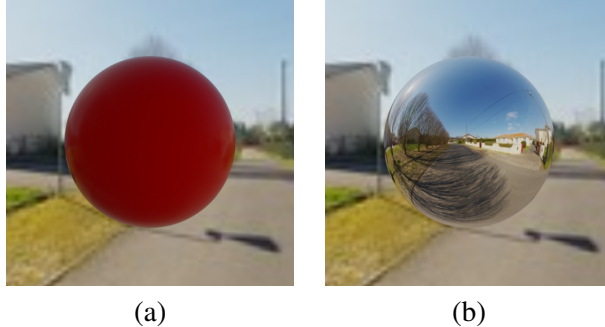


Figure 4.4: (a). A **red** diffuse sphere; (b). a **red** specular sphere. The surface reflects light in a mirror-like way, showing a distorted environment. Since no diffuse reflection exists, the colour of the surface is no longer visible.

4.2.4 Roughness

Roughness, which refers to the microscopic shape characteristics of a surface, contributes to the way in which light is reflected off of a surface. A smooth surface may reflect incident light in a single direction, while a rough surface may scatter the light in various directions. Thus, variations in microscopic surface geometry can cause specular reflections to be scattered, blurring the image of the environment in an amount proportional to surface roughness. We need prior knowledge of the microscopic surface irregularities, or a model of the surface itself, to determine the reflection of incident light.

Possible surface models are divided into 2 categories: surfaces with exact known profiles and surfaces with random irregularities. An exact profile may be determined by measuring the height at each point on the surface by means of a sensor such as the stylus profilometer. This method tends to be cumbersome and impractical, hence, it is more reasonable to model the surface as a random process, where it is described by a statistical distribution of either its height above a certain mean level, or its slope with respect to its mean (macroscopic) slope. We use the second statistical approach as the representation of roughness.

4.2.5 Perception of properties

Different materials can be visually distinguished because they structure light in a particular, characteristic way. The way light is structured depends heavily on the shape of object, reflectance and transmittance properties of material, and illumination field. This process is called the ‘forward optics’ (image formation) process. The material perception problem is, in some sense, the ‘inverse optics’ problem: determining what combination of surface geometry, surface material, and illumination field generated a given image. Thus, in order to recover the reflectance properties of materials, the visual system must somehow disentangle the contributions of the illumination field and geometry. This is arguably the central problem of material perception, though the answer is currently far from clear. But our intuition and many empirical studies support the view that humans are exceptional at material perception.

Everyday experience suggests that, human’s visual system are extremly good at estimating material properties. We can effortlessly distinguish numerous different categories of material: textiles, stones, liquids, foodstuffs, and so on, and can recognize many specific materials within each class such as silk, wool and cotton. Besides, being able to visually distinguish between materials and infer their properties by sight, is invaluable for many tasks. For instance, when determining edibility, we can make subtle visual judgements of material properties to determine whether fruit is ripe, whether soup has bee left to go cold or whether bread is going stale [16]. There are numerous experimental evidence to support this intuition. For example, Sharan et al. have shown that subjects can identify a wide range of materials from photographs even with brief presentations. Fleming et al. showed subjects photographs of materials from different categories and asked them to rate various subjective qualities, such as hardnessss, glossiness and prettiness. Even though subjects were not explicitly informed that the samples belonged to different classes, the subjective ratings of the individual samples were systematically clustered into categories, suggesting that subjects could theoretically classify materials through visual judgements of their properties.

Empirical studies have focused on the visual estimation of specific properties of materials, such as glossiness, translucency or surface roughness. For instance,

on the topic of glossiness, Nishida and Shinya showed that subjects can judge the specular reflectance of computer simulated glossy surfaces [45], and Fleming et al. showed that this ability generalizes across differences in lighting, as long as the illumination has statistical structure that is typical of the natural environment [17]. Fleming argued that the visual system does not actually estimate physical parameters of materials and objects, for instance, parameters of a reflectance model. Instead the brain is remarkably adept at building ‘statistical generative models’ that capture the natural degrees of variation in appearance between samples [16]. Though there is currently no universally accepted theory on visual perception of material, both our intuition and empirical results do suggest that human are exceptionally good at ‘estimating’ material properties.

Despite its subjective ease, material perception still poses the visual system with some unique and significant challenges, because a given material can take on many different appearances depending on the lighting, viewpoint and shape. Thus, we provide a *generative* approach to visual perception: a simulation software is used to generate images of a synthetic object with varied property settings to aid the estimation of properties. The user can choose an illumination field and object shape that is closest to the real-world enviriontment and object. Then a “try-and-see” approach was taken to obtain the parameters. More specifically, the user would change the value of each property and see if the rendered result resem-bles the real object. A similar approach can be found in [8] where Berkiten and Rusinkiewicz used a synthetic dataset to find the contributing factors of various Photometric Stereo algorithms.

The lightness of the object is controlled by the albedo value. Albedo is defied as the ratio of reflected light with respect to incident light. The albedo is determined by the value channel of HSV colour space. To determine the specularity and roughness of the object, we experiment with varying parameters to get the most realistic image. We demonstrate the process using the following example data ‘vase’, as shown in Figure 4.5.

4.2.6 Summary

The model and corresponding rerpesentations are shown in Table 4.2.

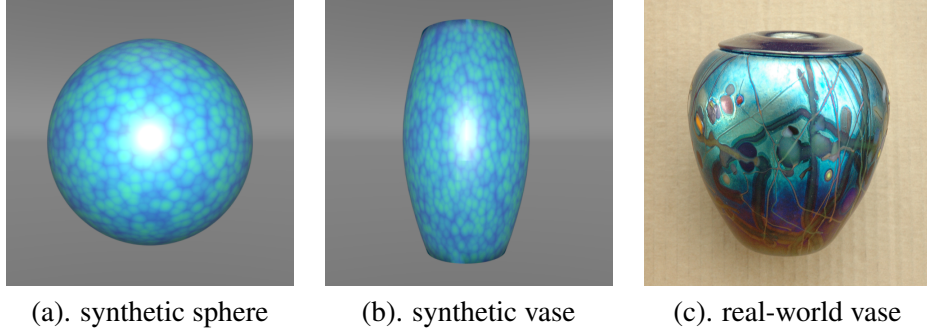


Figure 4.5: The UI for determining the property settings, including albedo, specular, and roughness of the surface. In this case shown above, the problem condition is: texture (0.8), albedo (0.8), specular (0.2), roughness(0.2). (a) demonstrates the effect of the property settings on a sphere, (b) on a teapot, and (c) shows the real-world object.

Model	Representation
Texture	<i>Texture randomness</i>
Lightness	<i>Diffuse albedo</i>
Specularity	<i>Specular reflectance</i>
Roughness	<i>SD of facet slopes</i>

Table 4.2: A Model and corresponding representations of the 3D reconstruction problem.

4.3 Expression

Now that we have a proposed model and representations of 3D reconstruction problem, we can express the four proposed problem conditions using this description. Given that all perceived estimates would likely be low resolution from users, we use three discrete scales to parameterize these properties: *low* (0.2), *medium* (0.5), and *high* (0.8). The expression of the reconstruction problem is shown in table 4.3.

Object	Texture	Albedo	Specular	Rough	Label
Class 1	low/med	high	low/med	high	Tl-B-D-R
Class 2	low/med	high	high	low/med	Tl-B-M-S
Class 3	high	high	low/med	high	T-B-D-R
Class 4	high	high	high	low/med	T-B-M-S

Table 4.3: Expression of the reconstruction problem for the four problem conditions proposed in Section 3.

Chapter 5

A Mapping of 3D Reconstruction

Most vision work focuses on developing algorithmic novelties, and as we have mentioned, very few investigate the rigorous conditions under which the algorithms themselves work. Thus, this knowledge is only known empirically, without a rigorous definition of the application domain or problem conditions. This relation between problem space and algorithms (termed as *mapping*) is one of the key components of the interpreter, and is responsible for selecting one of the best possible algorithms based on described problem condition. This section builds upon the 3D description proposed in Chapter 4, and attempts to find the problem conditions surrounding each algorithm empirically.

To achieve this goal, we need a dataset to evaluate the performance of each algorithm under varied problem conditions, which is not available since most 3D benchmarks, to the best of our knowledge, focus on one specific class of algorithms. For example, the Middlebury dataset targets MVS algorithms [54], and the ‘DiLiGenT’ dataset targets Photometric Stereo algorithms [56]. This makes such benchmarks only suitable for evaluation of within-category algorithms. Besides, there are no datasets with objects that cover a range of properties of materials and geometry. The reason for the lack of such a dataset is that it is practically impossible to change one property, e.g., surface texture, material, and so on, while fixing others when creating a real-world dataset.

In response to these challenges, we use synthetic datasets created by physical-based rendering software (Blender), to evaluate the 3D reconstruction algorithms.

Our dataset includes a collection of images of a scene under different materials and lighting conditions. The camera/projector’s intrinsic and extrinsic parameters are computed directly from the configurations of the synthetic setup, and the ground truth, including the 3D model point cloud and normal map, are generated directly from Blender.

5.1 Synthetic setup

We use Blender’s physical-based rendering engine, Cycles, to generate the synthetic datasets. For each technique, the configuration of the camera remains fixed. The image resolution is 1280×720 , with a focal length of 35mm or 1400pix . The synthetic setups are shown in Table 5.1, and some example synthetic images generated using the setups are shown in Figure 5.1.

Method	Hardware number	Arrangement
MVS	41 camera	5 rings, each having 1, 8, 8, 12, 12 camera
PS	1 camera+25 lights	4 rings, each having 1, 8, 8, 8, 8 light sources
SL	1 camera&projector	baseline angle: 10°

Table 5.1: Summary of synthetic setups.

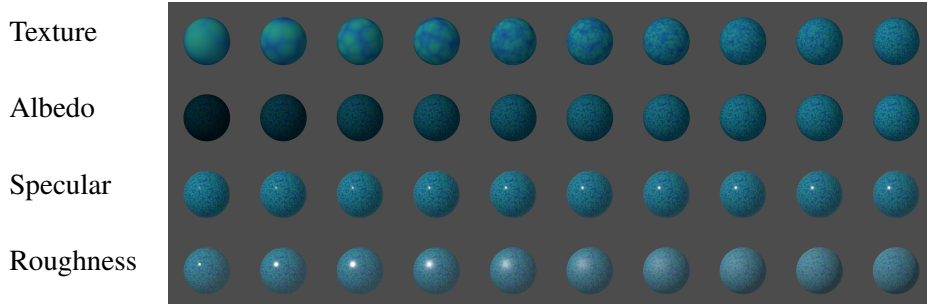


Figure 5.1: Example synthetic images. The value of each property ranges from 0.1 to 1.

5.2 Selected and baseline methods

We have selected one representative algorithm from three major classes of algorithms presented in Chapter 3: the PMVS proposed in [20], the example-based Photometric Stereo proposed in [26], and the Gray-code Structured Light technique. See Table 5.2 for a summary of the selected algorithms. The current implementation of SL projects both column and row patterns, and depth values are computed using these two kinds of patterns individually. A depth consistency step is performed to reject erroneous triangulations.

Technique	Summary
PMVS	Patch-based, seed points propagation MVS.
EPS	Example-based Photometric Stereo.
GSL	Gray code Structured Light technique.
VH	Volumetric Visual Hull.
LLS-PS	Linear least squares Photometric Stereo.

Table 5.2: Summary of the selected and baseline algorithms for the interface, and the corresponding working conditions in theory.

We use two baseline approaches to compare our results: Visual Hull and a simple linear least squares based Photometric Stereo (LLS-PS). We use Visual Hull since it works relatively well as long as the silhouette of the object can be reliably extracted, thus being insensitive to material properties. In addition, the true scene is always enclosed by the reconstruction result, so the outcome is always predictable. We use LLS-PS to evaluate Photometric Stereo algorithms. However, there is currently no such PS algorithms that work reasonably well under a variety of conditions. Thus, we run this baseline algorithm under the optimal condition to ensure a best possible result.

5.3 Quantitative measures

We use the metrics proposed in [54] to evaluate MVS and SL algorithms. More specifically, we compute the accuracy and completeness of the reconstruction. For accuracy, the distance between the points in the reconstruction R and the nearest

points on ground truth G is computed, and the distance d such that $X\%$ of the points on R are within distance d of G is considered as accuracy. A reasonable d value is between $[3, 5]mm$, and X is set as 95. The lower the accuracy value, the better the reconstruction result. For completeness, we compute the distance from G to R . Intuitively, points on G are not “covered” if no suitable nearest points on R are found. A more practical approach computes the fraction of points of G that are within an allowable distance d of R . Note that as the accuracy improves, the “accuracy value” goes down, whereas as the completeness improves, the “completeness value” goes up.

For photometric stereo, depth information is lost since only one viewpoint is used. Thus, the previous metrics are not applicable. Here we employ another evaluation criteria that is widely adopted, which is based on the statistics of angular error. For each pixel, the angular error is calculated as the angle between the estimated and ground truth normal, i.e., $\arccos(n_g^T n)$, where n_g and n are the ground truth and estimated normals respectively. In addition to the mean angular error, we also calculate the standard deviation, minimum, maximum, median, first quartile, and third quartile of angular errors for each estimated normal map.

5.4 Effective Problem Domain (EPD)

The greatest challenge in constructing a mapping from problem space to algorithms is the large variations in shapes and material properties, which results in a problem space that is too large to cope with. Suppose there are N properties, each with L discrete levels, then there are in total L^N different problem conditions. Thus, the first step, discussed in Section 5.4.1, 5.4.2, 5.4.3, is to reduce the dimensions of problem space by establishing the *effective problem domain* EPD = $\text{set}(p_i^j)$, where $i \in \{0, \dots, L - 1\}$, and $j \in \{0, \dots, N - 1\}$, which consists of only effective properties. Then, Section 5.5.1, 5.5.2, 5.5.3 evaluate performance of selected algorithms within the corresponding EPD.

A naive way of finding the *effective properties* would be evaluating algorithmic performance by changing one property at a time. However, this approach ignores the dependency between properties, i.e., the effect of property A might be insignificant when property B is absent. Thus, we investigate the pairwise relation between

any two properties, thus two properties are chosen while the rest are fixed, the configurations of the problem conditions are shown in Table 5.3

Cond.	Texture	Albedo	Specular	Roughness
(a)	[0.2, 0.8]	[0.2, 0.8]	0.0	0.0
(b)	[0.2, 0.8]	0.8	[0.2, 0.8]	0.0
(c)	[0.2, 0.8]	0.8	0.0	[0.2, 0.8]
(d)	0.8	[0.2, 0.8]	[0.2, 0.8]	0.0
(e)	0.8	[0.2, 0.8]	0.0	[0.2, 0.8]
(f)	0.8	0.8	[0.2, 0.8]	[0.2, 0.8]

Table 5.3: Problem conditions for establishing the *effective problem domain* of all selected algorithms. For instance, cond. (a) considers texture and albedo while specularity and roughness are fixed. The value of both varying properties range from 0.2 to 0.8.

5.4.1 EPD: PMVS

We investigate the impact of each property on the performance of PMVS in terms of accuracy and completeness under varied combinations of properties. The settings of these properties are listed in Table 5.3.

(a) Texture and Albedo texture has a positive effect on the reconstruction in terms of accuracy and completeness, while the effect of albedo is negligible.

(b) Texture and Specularity specularity has a negative effect on both the accuracy and completeness of the reconstruction. However, the level of impact varies as the texture varies. More specifically, the effect of specularity is more substantial on a less textured surface, as shown in Figure 5.2 (b). This can be explained as follows: the specular lobe can only be observed by cameras positioned and oriented towards the specular lobe, such as camera V_2 shown in Figure 5.3 (a) and (c). Cameras positioned otherwise would observe the true surface, such as camera V_1 shown in Figure 5.3 (a) and (b). The algorithm would then exploit the texture information provided by views like V_1 , and thus would be able to reconstruct a specular surface.

(c) Texture and Roughness roughness doesn't have a significant effect on the results.

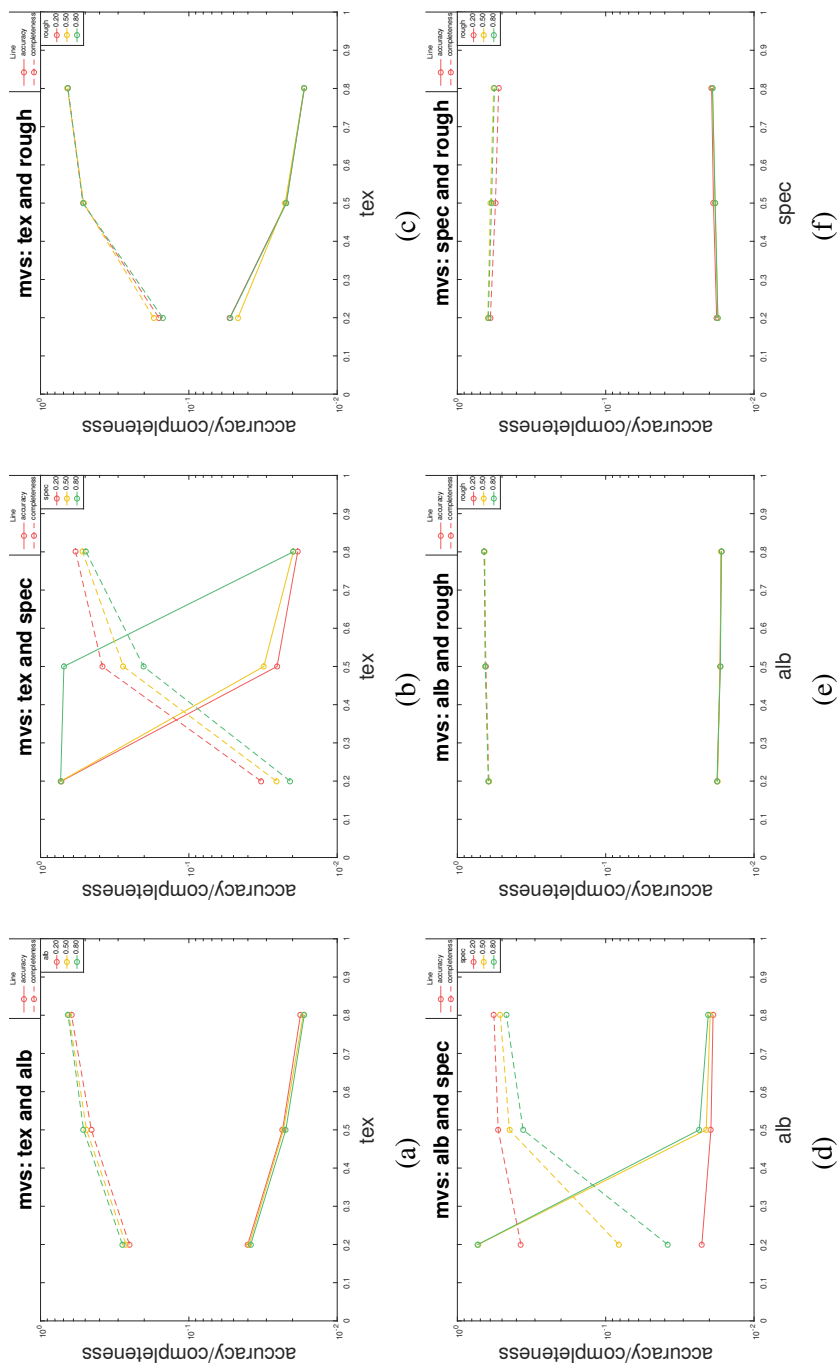


Figure 5.2: Performance of PMVS under six pairwise conditions. For instance, (a) shows the performance under changing *texture* and *albedo* values, while the others are fixed. The property values are set based on settings in Table ??.

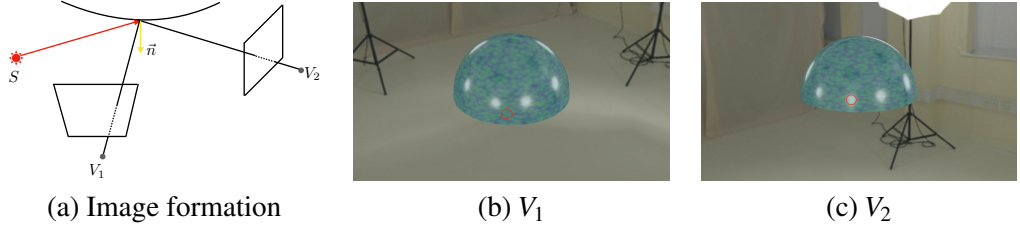


Figure 5.3: (a) shows the reflection of light off a specular surface. V_1 received the diffuse component while V_2 receives the specular component. (b), (c) shows the images observed from these two views. The specular area (red circle) observed in V_2 is visible in V_1 .

(d) Albedo and Specular albedo has a positive effect whereas specular has a negative effect on the reconstruction. Furthermore, the positive effect of albedo is more significant on a higher specular surface while the negative effect of specular is far more substantial on a lower albedo surface. This can be explained as follows: according to the energy conservation law, as the specular component increases, the diffuse component decreases, resulting in a less discernible diffuse area. See Figure 5.4 (a)-(c). Increasing the diffuse albedo can counteract the effect of specularity and make the texture visible again. See Figure 5.4 (d)-(f).

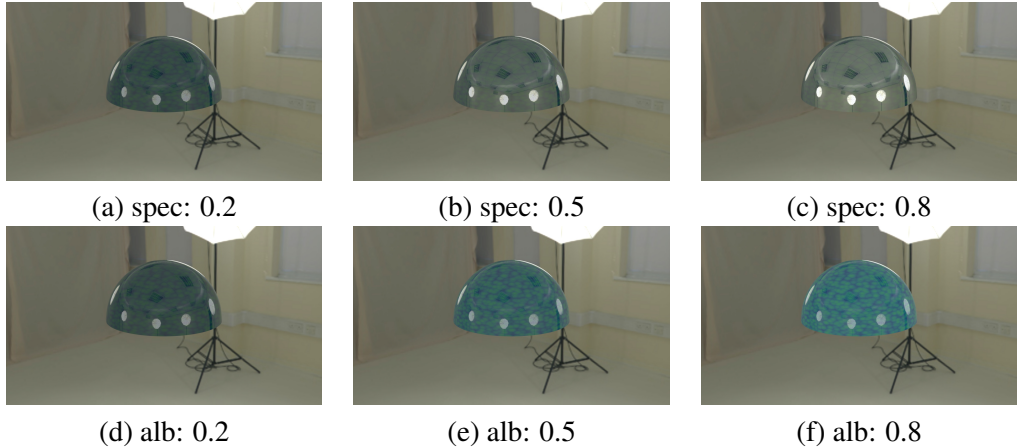


Figure 5.4: (a)-(c). The albedo is set as 0.2, (d)-(f). The specularity is set as 0.2. According to energy conservation, as the specular component increases, the diffuse component decreases.

(e) Albedo and Roughness albedo and roughness have a negligible effect on the results.

(f) Specular and Roughness surface roughness can effectively diminish the specular component and make the surface appear more diffuse. Thus, in theory, roughness should have a positive impact on the reconstruction. However, since specularity is only effective on surface with medium level texture, see Figure 5.2 (b), then roughness is only effective in this case as well. Further, since higher specular, high roughness surfaces visually resemble lower specular surfaces, and achieve similar reconstruction results as well, it makes sense to incorporate the effect of roughness to specularity, and omit roughness for simplicity.

Effective Properties: PMVS

The effective properties of PMVS are: texture, albedo, and specular, as shown in Table 5.4. Interestingly, we discovered that specularity has a more substantially negative impact on less textured, lower albedo surfaces. For instance, high specularity does not have a severely negative impact on highly textured surfaces.

Metric	Texture	Albedo	Specular	Roughness
Accuracy	✓	✓	✓	✗
Completeness	✓	✓	✓	✗

Table 5.4: The *effective problem domain* of PMVS in terms of accuracy and completeness.

5.4.2 EPD: EPS

We investigate the impact of each property on the performance of example-based PS in terms of angular error under varied combinations of properties. The settings of the properties are listed in Table 5.3.

(a) Texture and Albedo texture has no significant effect while albedo has a positive effect on normal estimation.

(b) Texture and Specularity texture has no effect while specularity has a negative effect on normal estimation, which is manifested by the increased interquartile range and skewness. The explanation is as follows: normals in the specular re-

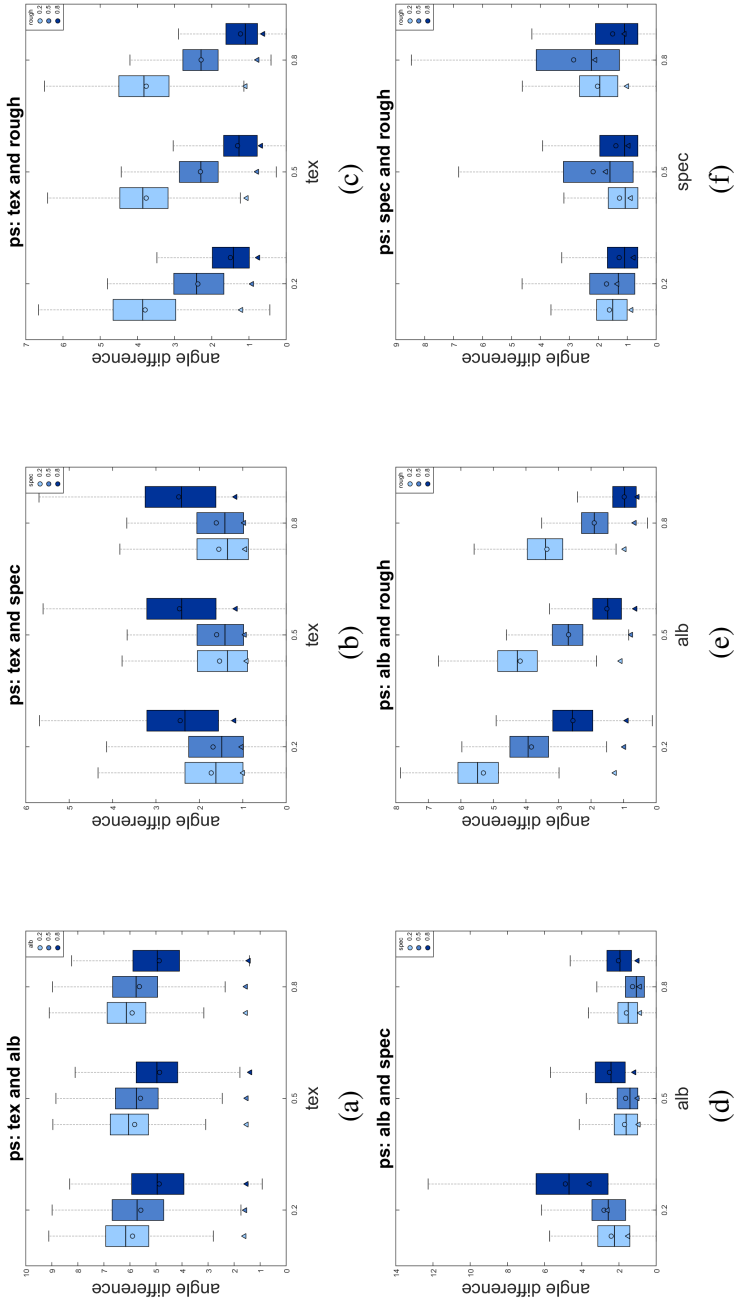


Figure 5.5: Performance of Example-based PS under six pairwise conditions. For instance, (a) shows the performance under changing *texture* and *albedo* values. The property values are assigned based on the settings in Table ?? (a).

gions are poorly estimated while the rest of the surface is reliably estimated, as shown in Figure 5.6. This explains the increased mean and interquartile values as shown in Figure 5.5 (b).

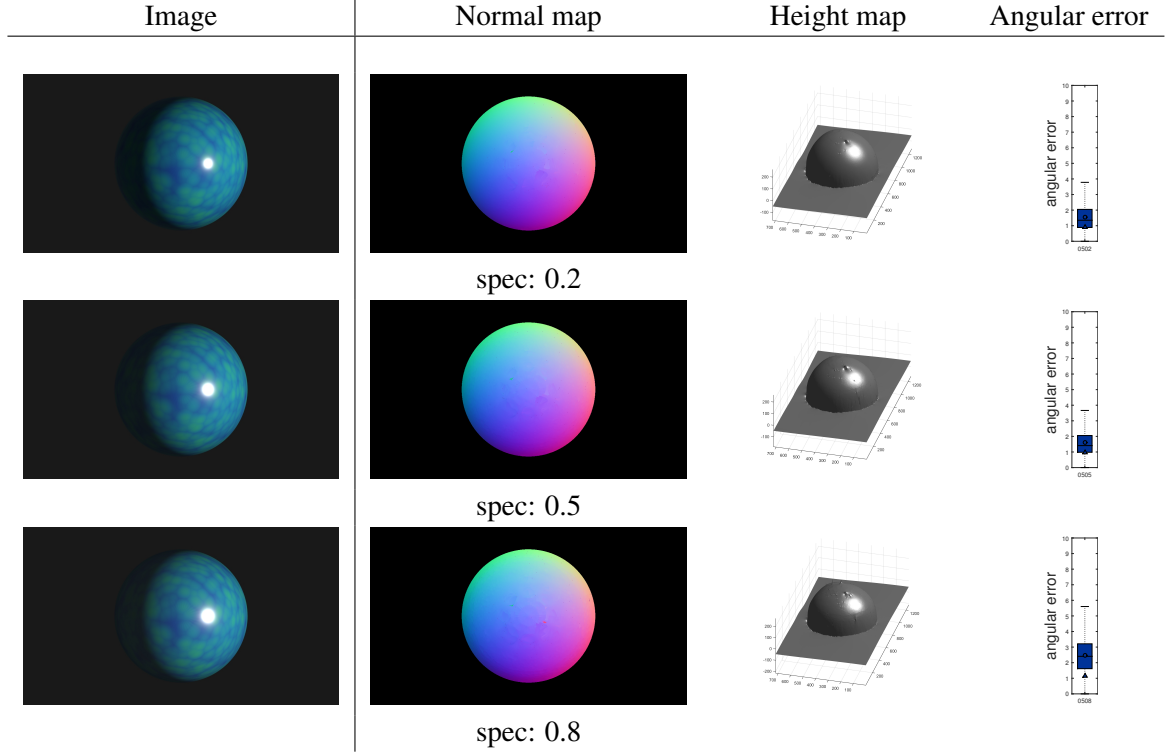


Figure 5.6: (a)-(c). The texture is set as 0.5. The estimated normal map and recovered surface becomes consistently worse as the specular level rises, which is consistent with the quantitative results from Figure 5.5 (b).

(c) Texture and Roughness texture has no effect while roughness has a positive effect on normal estimation.

(d) Albedo and Specular the albedo has a positive impact on normal estimation (see Figure 5.7 (a)-(c)), whereas the specularity has a negative impact on normal estimation (see Figure 5.7 (d)-(f)).

(e) Albedo and Roughness both albedo and roughness have a positive effect on normal estimation.

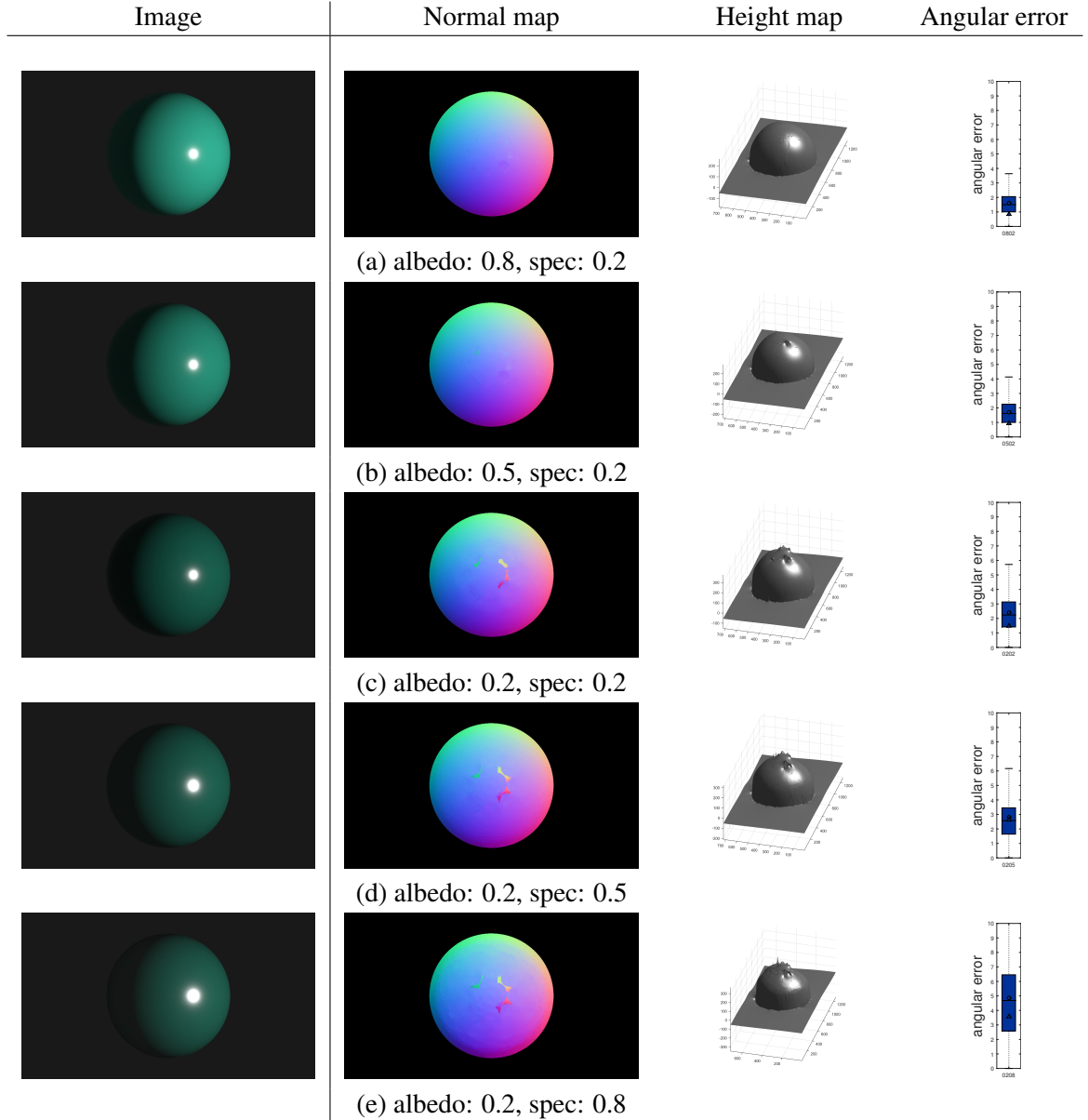


Figure 5.7: According to energy conservation, as the specular component increases, the diffuse component decreases. (a)-(c): the estimated normal map and recovered height map become consistently worse as the albedo decreases; (c)-(e): the estimated normal map and recovered height map become consistently worse as the specularity increases.

(f) Specular and Roughness specularity has a negative impact on normal estimation, while the effect of roughness is more complicated. We observed that the reconstruction becomes worse for medium roughness, which is counter-intuitive at first sight. However, we argue that it's because the roughness is not strong enough to counteract the specular component, causing a smoothed and blurred specular region with larger area, thus leading to a poorer normal estimation. See Figure 5.8 for visual examples.

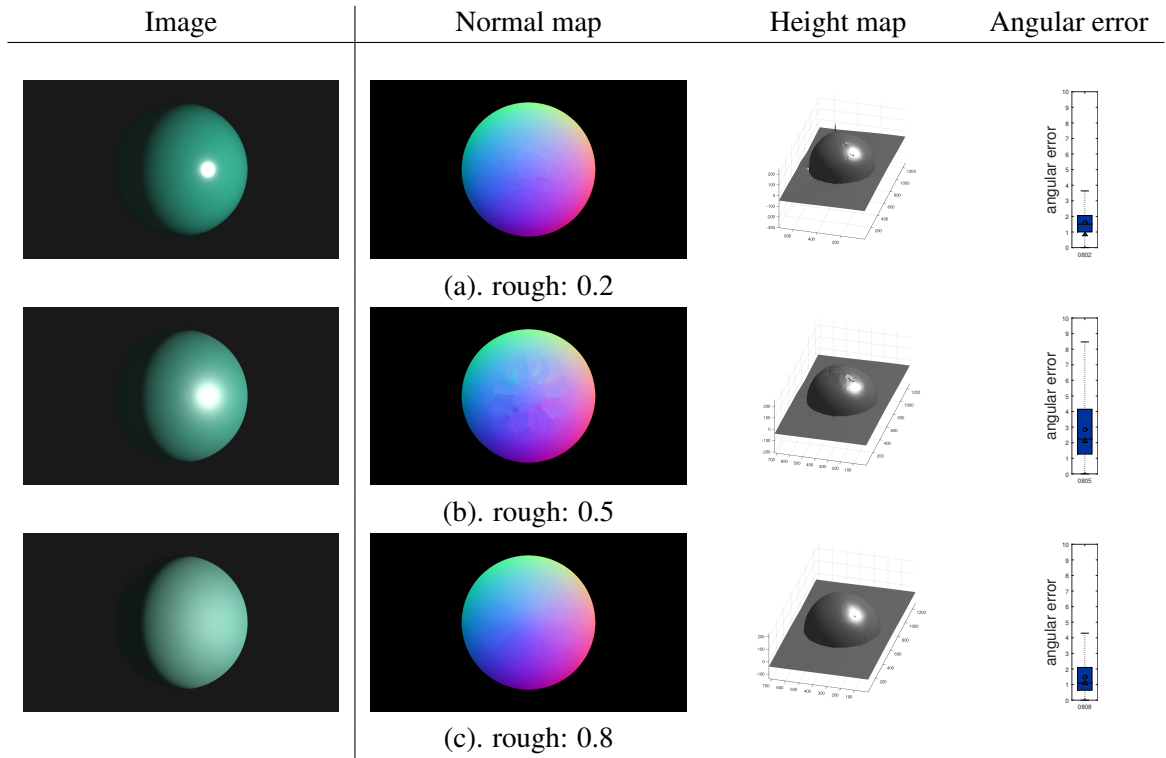


Figure 5.8: The effect of roughness on PS. Albedo is set as 0.8, and specular is set as 0.8. (b) demonstrates that a medium level roughness would lead to worse normal estimation since it blurs the specular lobe.

Effective Properties: EPS

The properties that have an impact on EPS are: albedo, specularity, and roughness, as shown in Table 5.5. Interestingly, we have discovered that medium level rough-

ness can have a negative impact on normal estimation by blur the specular lobe, as shown in Figure 5.8.

Metric	Texture	Albedo	Specular	Roughness
Angle difference	✗	✓	✓	✓

Table 5.5: The *effective problem domain* of EPS in terms of the *angular error*.

5.4.3 EPD: GSL

We investigate the impact of each property on the performance of Gray-code SL in terms of accuracy and completeness under a varied combination of properties. The settings of properties are listed in Table 5.3.

- (a) **Texture and Albedo** texture has no significant effect, whereas albedo has a positive effect on completeness. Both properties have no significant effect on accuracy.
- (b) **Texture and Specular** texture has no significant effect whereas specular has a negative effect on completeness. Both properties have no significant effect on accuracy.
- (c) **Texture and Roughness** neither texture nor roughness has a significant effect on accuracy and completeness.
- (d) **Albedo and Specularity** albedo has a positive effect (see Figure 5.10 (a)-(c)) whereas specularity has a negative effect on completeness (see Figure 5.10 (d)-(f)). Interestingly, similar to EPS, the positive effect of albedo gets more significant with higher specularity while the negative effect of specularity becomes less substantial as albedo increases (see Figure 5.9 (d)). Neither property has a significant effect on accuracy.
- (e) **Albedo and Roughness** albedo has a positive effect, whereas roughness has a negligible effect on completeness. Both properties have no significant effect on accuracy.
- (f) **Specular and Roughness** specular has a negative effect (see Figure 5.11 (a)-(c)). Interestingly, the effect of roughness also resembles that of EPS, i.e., medium level roughness has a negative impact on completeness (see Figure 5.11 (d)-(f)). Neither property has a significant effect on accuracy.

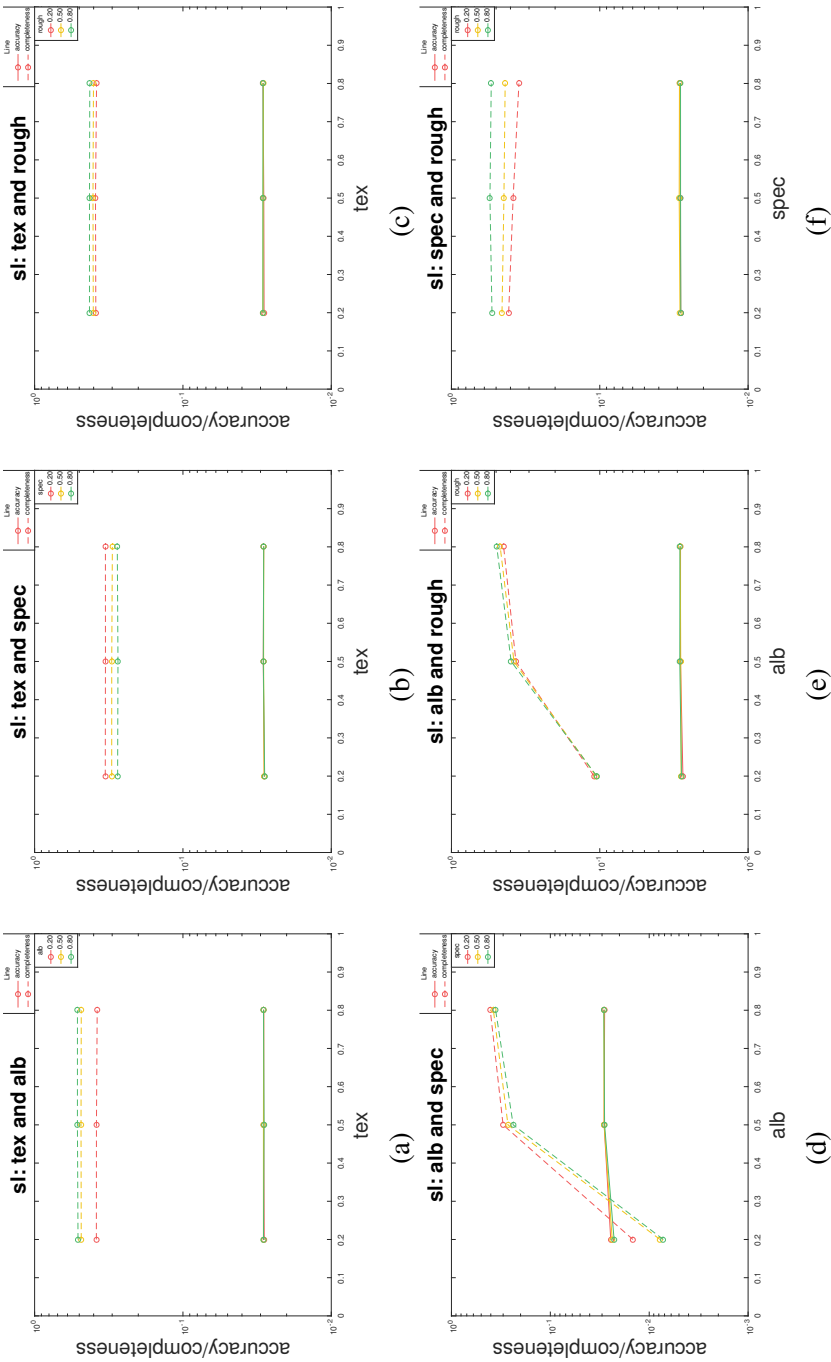


Figure 5.9: Performance of Gray-encoded SL under six pairwise conditions. For instance, (a) shows the performance under changing *texture* and *albedo* values. The property values are assigned based on settings in Table ?? (a).

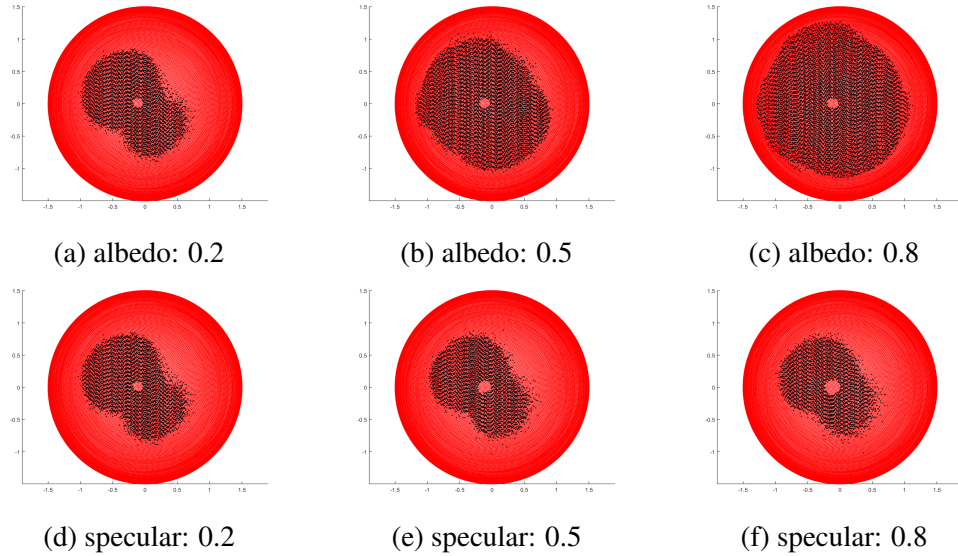


Figure 5.10: (a)-(c): the specular is set as 0.2, albedo has a positive effect on completeness; (d)-(e): the albedo is set as 0.2, specular has a negative effect on completeness.

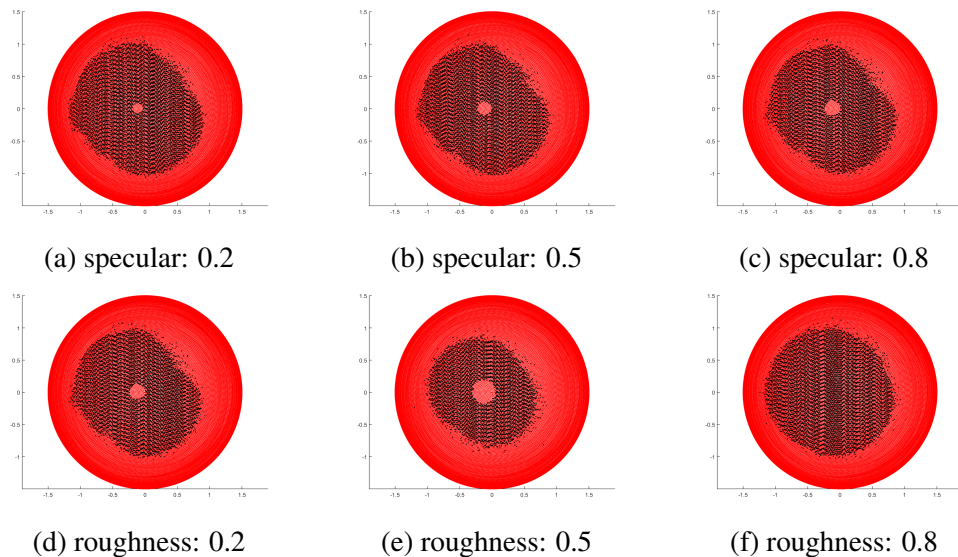


Figure 5.11: (a)-(c): the roughness is set as 0.2, and specular has a negative effect on completeness; (d)-(e): the specular is set as 0.8, roughness has a positive effect on completeness.

Effective Properties: GSL

The properties that have an effect on the GSL are: texture, albedo, specular, as shown in Table 5.6. The albedo has a more significant impact with lower specularity, while specularity has a more substantial impact with low albedo. Roughness can cause a blurred specular region, thus leading to decreased completeness.

Metric	Texture	Albedo	Specular	Roughness
Accuracy	✗	✗	✗	✗
Completeness	✗	✓	✓	✓

Table 5.6: The *effective problem domain* of GSL in terms of accuracy and completeness.

5.5 Mapping Construction

Once we have discovered the EPD, the algorithm is evaluated solely within the EPD. Since there are three *effective properties*, each with 3 discrete levels, thus there are 27 problem conditions. We present the quantitative results of the conditions as follows: results are divided into three plots. In each plot there are one fixed property P_1 , and two changing properties P_2 and P_3 . To have a better understanding of the pairwise relation between any two properties, each *effective property* would be chosen as P_1 once. Therefore, we end up with three groups of graphs, each consisting of three plots, as shown in Figure 5.12, 5.13, and 5.14.

5.5.1 Mapping: PMVS

The performances of PMVS under different problem conditions are shown in Figure 5.12, along with the performance of the baseline method. We make the following observations from the results: accuracy and completeness improves consistently as the *texture* level increases. Accuracy and completeness results deteriorate consistently as *specularity* increases, and this negative impact is most significant when texture level is medium or albedo value is low. The effect of *albedo* on a surface with low texture is negligible. However, albedo has a noticeably more significant positive impact on completeness as the texture of a specular surface increases.

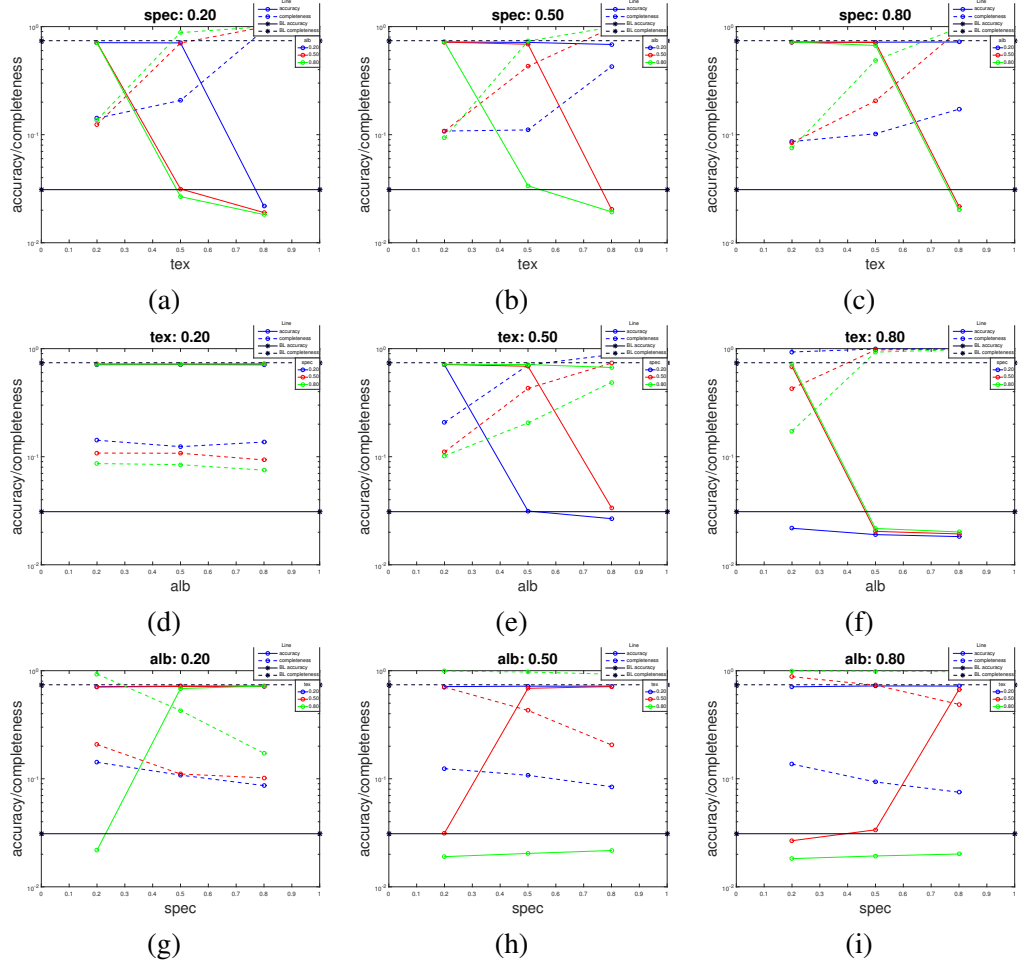


Figure 5.12: Performance of PMVS under varied conditions of changing property values. The baseline method serves as the guidelines to determine the performance of PMVS.

We derive from the results, as shown in Figure 5.12, the problem conditions under which PMVS performs reliably, as shown in Table 5.7. The reliability is determined by comparing to the results of the baseline method.

Metric	Texture	Albedo	Specular	Roughness
Accuracy	0.5	0.5	0.2	-
&Completeness	0.5	0.8	0.2	-
	0.5	0.8	0.5	-
	0.8	0.2	0.2	-
	0.8	0.5	0.2	-
	0.8	0.8	0.2	-
	0.8	0.5	0.5	-
	0.8	0.8	0.5	-
	0.8	0.5	0.8	-
	0.8	0.8	0.8	-

Table 5.7: The working problem conditions of PMVS in terms of the two metrics *accuracy* and *completeness*.

5.5.2 Mapping: EPS

The performances of example-based PS under different problem conditions are shown in Figure 5.13, along with the result of the baseline method. We make the following observations from the results: *albedo* has a consistently positive effect on normal estimation; *specularity* has a consistently negative impact on normal estimation; and medium level *roughness* will lead to a worse normal estimation.

We derive from the results, as shown in Figure 5.13, the problem conditions under which EPS performs reliably, as shown in Table 5.8. The reliability is determined by comparing to the results of the baseline method.

5.5.3 Mapping: GSL

The performances of Gray-code SL under different problem conditions are shown in Figure 5.14, along with the results of the baseline method. Note that only a portion of the object is visible because of one viewpoint. The percentage of the visible surface (α) varies from object to object, and is approximated by the completeness

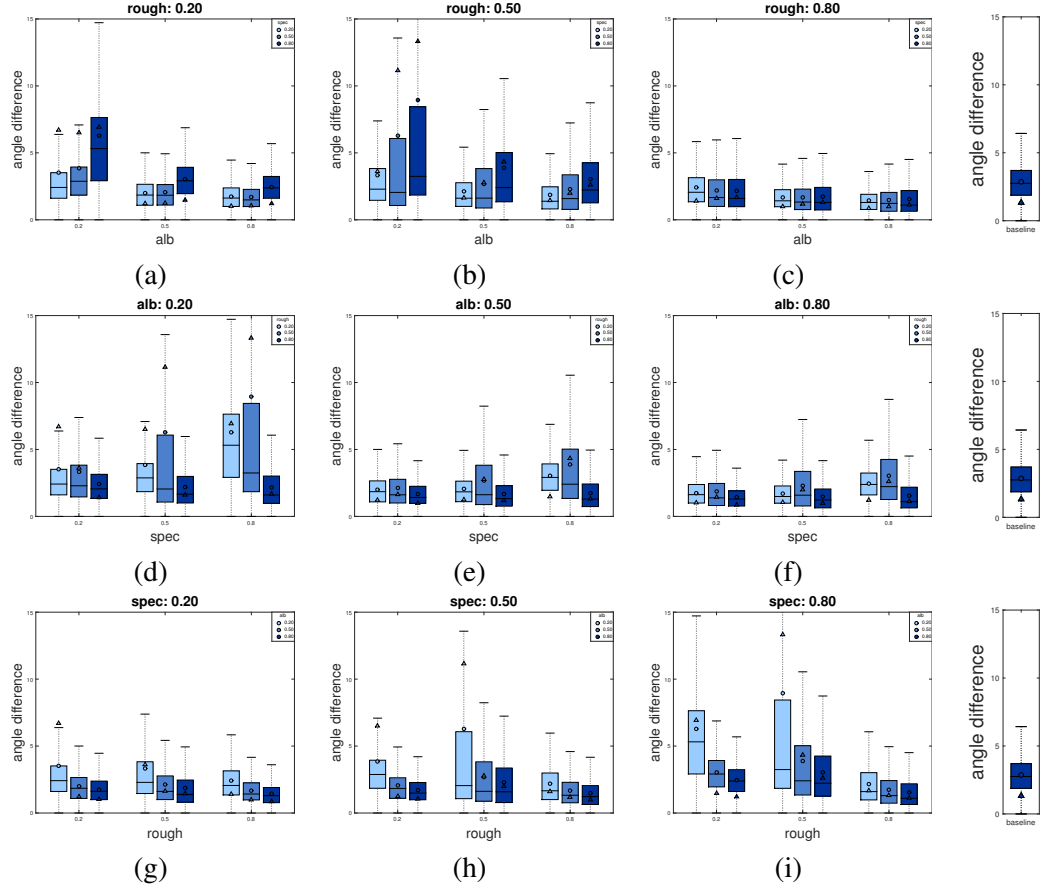


Figure 5.13: Performance of EPS under varied conditions of changing property values. Varied statistical measures of angular error are compared to the baseline method to determine the performance of EPS.

value obtained under the optimal reconstruction condition. The performance of GSL is determined by comparing the completeness to *alpha* that of the baseline. We make the following observations: *albedo* has a consistently positive effect on completeness; medium level *roughness* has a negative effect due to a blurred specular region. In most case, *specularity* does have a negative effect on completeness, as shown in Figure 5.10 (d)-(f). However, we did notice in some cases that the completeness of the reconstruction improves as specular level increases. There are two contributing factors to completeness: 1) specularity decreases the complete-

Metric	Texture	Albedo	Specular	Roughness
Angle difference	-	0.2	0.2	0.8
	-	0.2	0.5	0.8
	-	0.2	0.8	0.8
	-	0.5	0.2	0.8
	-	0.5	0.5	0.8
	-	0.5	0.8	0.8
	-	0.8	0.2	0.2
	-	0.8	0.2	0.8
	-	0.8	0.5	0.2
	-	0.8	0.5	0.8
	-	0.8	0.8	0.2
	-	0.8	0.8	0.8

Table 5.8: The working conditions of example-based PS in terms of the metric *angular error*.

ness since the pattern can no longer be decoded in the glossy area, thus causing incomplete reconstruction; 2) large roughness can spread the specular lobe into a larger area, leading to a brighter surface, thus increasing the completeness of the reconstruction. These two contradicting factors together determine the completeness of the reconstruction. If the first factor is more substantial, the completeness will decrease whereas if the second factor is more significant, the completeness will increase.

We derive from the results, as shown in Figure 5.14, the problem conditions under which GSL could perform reliably by considering both the quantitative and qualitative results, as shown in Table 5.9. The reliability is determined by comparing to the results of the baseline method.

5.6 Evaluation of Mapping

The section validates that the derived mapping can be applied to objects with different shapes. Given the description of an object, we use all the implemented techniques for reconstruction, to see if the algorithms that give successful reconstructions in terms of quantitative or qualitative results are consistent to those chosen by the mapping. This evaluation intends to validate that the developed mapping can be

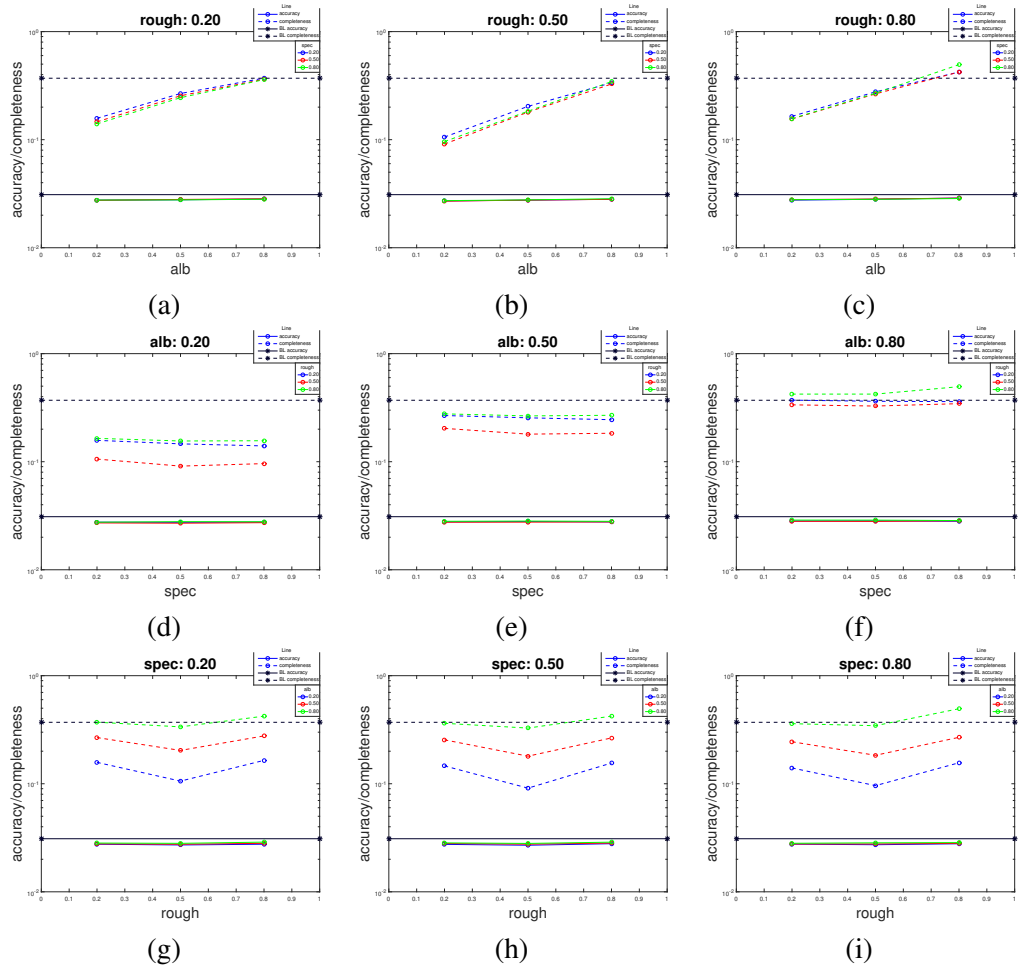


Figure 5.14: Performance of GSL under varied conditions of changing property values. The baseline method serves as the guideline to determine the performance of GSL.

Metric	Texture	Albedo	Specular	Roughness
Accuracy	-	-	-	-
Completeness	-	0.8	0.2	0.2
	-	0.8	0.5	0.2
	-	0.8	0.8	0.2
	-	0.8	0.2	0.8
	-	0.8	0.5	0.8
	-	0.8	0.8	0.8

Table 5.9: The condition matrix of Gray-code SL in terms of the two metrics *accuracy* and *completeness*.

applied to objects with different shapes, and demonstrate cases where it succeeds and fails

Is the mapping robust to changes of the shape of objects?

The sheer volume of object shapes and geometries makes it practically impossible to validate the applicability of the mapping to objects with varied shapes. Instead, we focus on one geometric property, surface concavity, that can have an impact on the results. We use three synthetic objects with varied degrees of concavity, and verify if the mapping is applicable under all circumstances, and when it would succeed or fail. We use synthetic data to verify the mapping since it would not be practical to change material properties using real world objects. We verify the robustness of the mapping following these two steps: 1) the successful algorithm(s) under each problem condition is identified based on the qualitative and quantitative results; 2) the reliable algorithms under each condition is consistent with the mapping results.

5.6.1 Synthetic Datasets

We use three objects with increasing degree of concavity, which are ‘bottle’, ‘knight’, and ‘king’, as shown in Figure 5.15. We select four property settings representing four object classes discussed in Chapter 4, as shown in Table 5.10. The results of the mapping are included in Table 5.10 as a reference. The reconstruction results are shown in Figure 5.16, 5.17, and 5.18. The mapping results are in the

first column, and the algorithms that produce successful results are labeled in the green box. The consistency of the algorithms in green box and the mapping results indicates the robustness of the mapping.

Class	Texture	Albedo	Specular	Rough	Metrics		
					Accuracy	Completeness	Ang error
(a)	0.2	0.8	0.2	0.8	GSL	GSL	EPS
(b)	0.2	0.8	0.5	0.2	GSL	-	-
(c)	0.8	0.8	0.2	0.8	PMVS, GSL	PMVS, GSL	EPS
(d)	0.8	0.8	0.5	0.2	PMVS, GSL	PMVS	-

Table 5.10: Property settings of the three testing objects: ‘bottle’, ‘knight’, ‘king’, which have increasing degree of concavity.

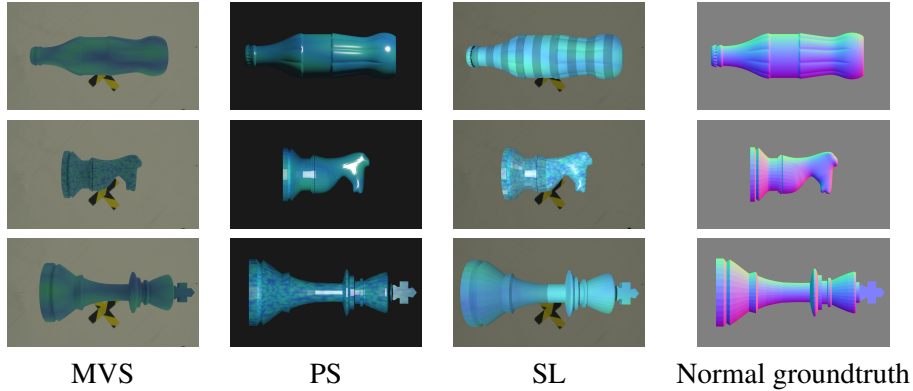


Figure 5.15: The synthetic dataset and groundtruth for the evaluation of the robustness of the mapping to concavity. Three objects with varied degrees of concavity are selected, each is configured with four properties settings listed in Table 5.10.

Data 1: bottle

The object ‘bottle’ has shallow concavities on the surface. Both quantitative and qualitative results are used to determine the successful algorithm under each problem condition. It’s clear that the algorithms achieve successful results are consistent with the mapping results under all problem conditions.

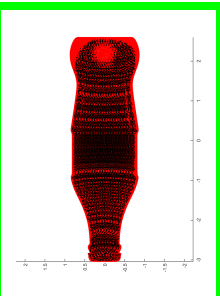
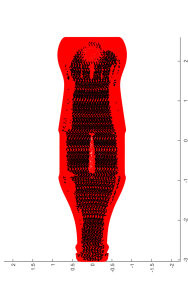
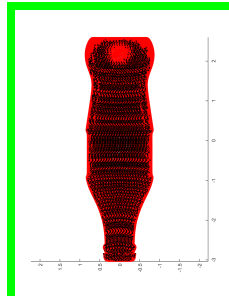
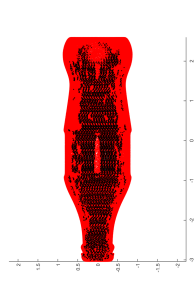
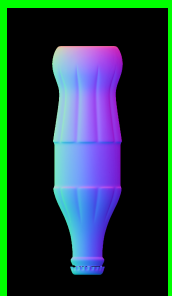
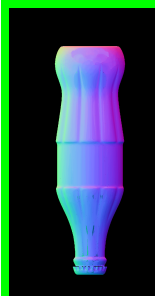
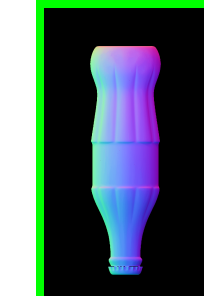
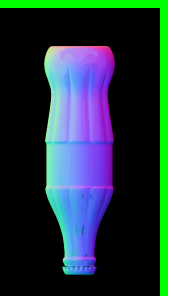
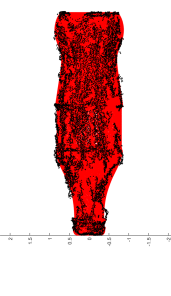
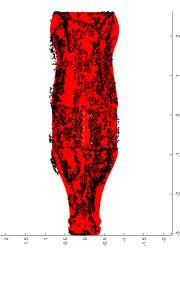
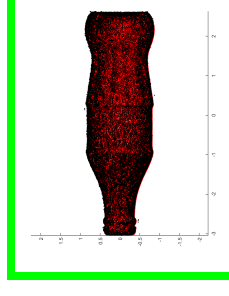
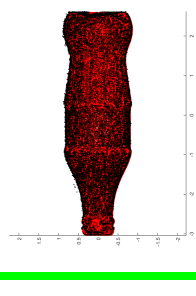
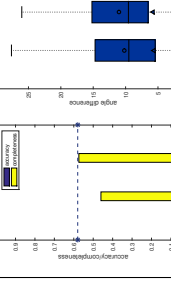
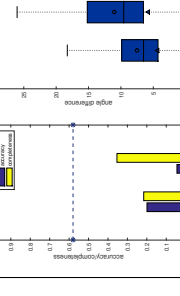
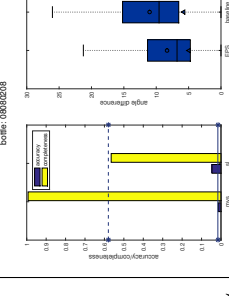
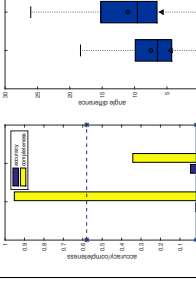
Mapping	Qualitative results				SL
	EPS, GSL	EPS	PMVS, EPS, GSL	PMVS, EPS	
(a). tex(0.2), alb(0.8), spec(0.2), rough(0.8)					
(b). tex(0.2), alb(0.8), spec(0.5), rough(0.2)					
(c). tex(0.8), alb(0.8), spec(0.2), rough(0.8)					
(d). tex(0.8), alb(0.8), spec(0.5), rough(0.2)					
MVS	PS	PS	PS	PS	SL

Figure 5.16: The first column shows the best algorithm chosen by the mapping. The quantitative and qualitative performance of each technique on the synthetic dataset is also shown. The red dots represent the ground truth while the black dots represent the reconstruction.

Data 2: knight

The second object is a knight chess piece with medium concavity. In this case, we can see that the results of PMVS and GSL are still consistent with the mapping. However, EPS fails to return reliable reconstruction in conditions of high specularity, such as (b) and (d), which is manifested by an increased standard deviation and the interquartile range of angular error. Thus, we claim that the mapping to PMVS and GSL, and that to EPS in case of low specularity are robust for surfaces with medium concavity.

Data 3: king

The last synthetic object is the king chess piece with high surface concavity. In the case of high concavity, results of PMVS and GSL are still consistent with those of the mapping. However, results of the EPS become inconsistent, which is a result of the cast shadow due to large concavity. Though the result of EPS under conditions (a) and (c) are still better than that of the baseline, the median angular error is above an acceptable threshold, which is 10° in most cases. We can see with more clarity from the qualitative results that the cast shadow on the ‘crown’ leads to completely inaccurate normal estimation, which is labeled in red rectangle. Thus, we claim that the mapping to PMVS and GSL remain robust for surfaces with large concavity.

5.6.2 Conclusion

We can conclude that the mapping to PMVS and GSL are robust with respect to concavity, whereas EPS is relatively more sensitive to concavity due to cast shadows. Therefore, we should redirect more research efforts to developing Photometric Stereo algorithms that can reliably deal with cast shadow so that they can be reliably applied to more complex shapes.

5.7 Summary

It is a non-trivial task to find a mapping from problem conditions to algorithms based on the description. By no means is the aforementioned approach the only

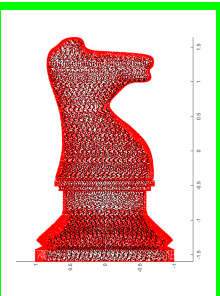
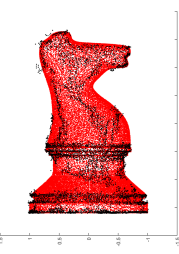
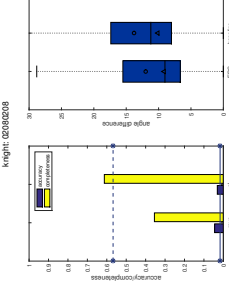
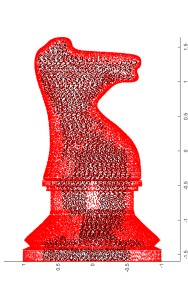
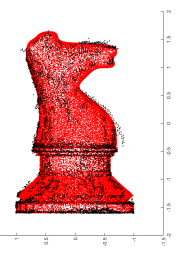
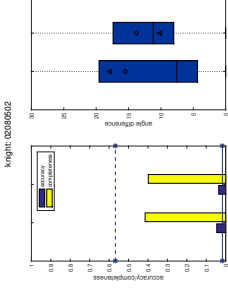
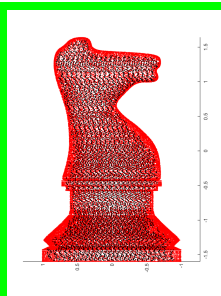
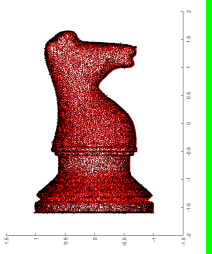
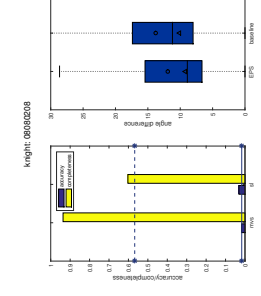
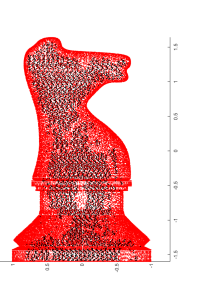
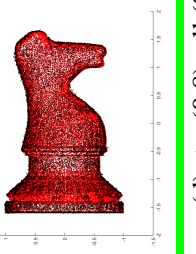
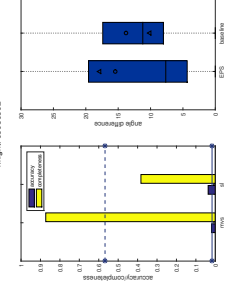
Mapping	Qualitative results				SL
	EPS, GSL	EPS	PMVS, EPS, GSL	PMVS, EPS	
EPS, GSL	   	   	   	   	(a). tex(0.2), alb(0.8), spec(0.2), rough(0.8)
EPS					
PMVS, EPS, GSL					
PMVS, EPS					

Figure 5.17: The first column shows the best algorithm chosen by the mapping. The quantitative and qualitative performance of each technique on the synthetic dataset is also shown. The red dots represent the ground truth while the black dot represent the reconstruction.

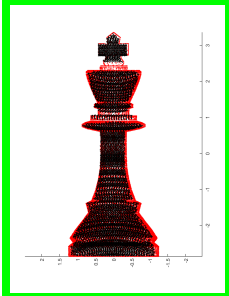
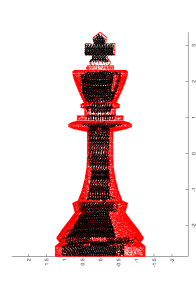
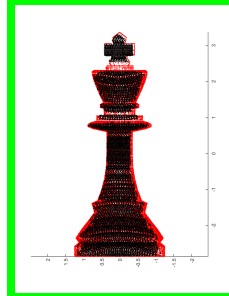
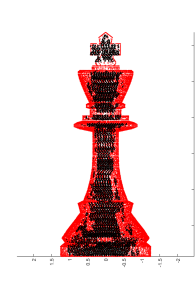
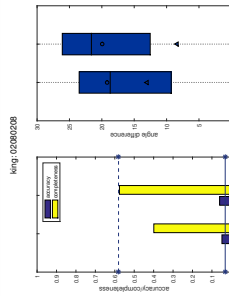
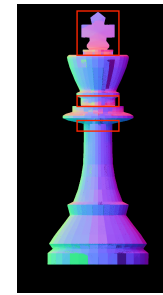
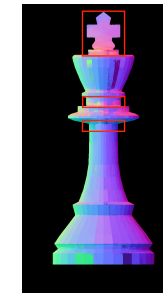
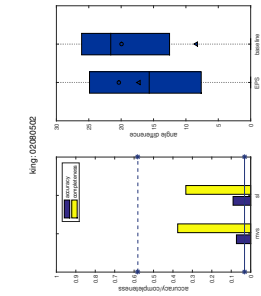
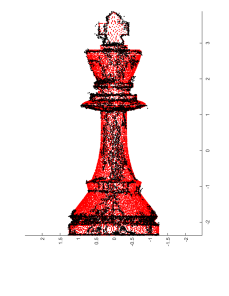
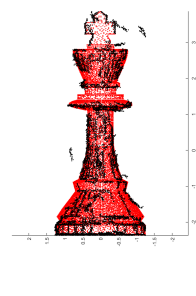
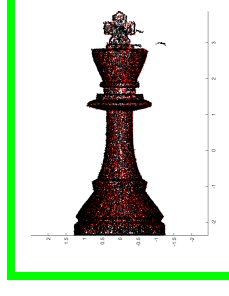
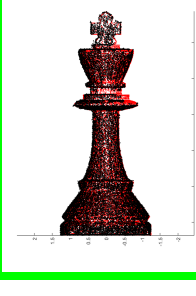
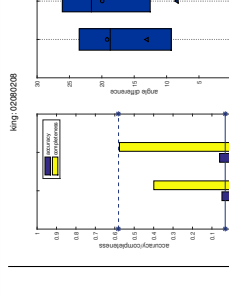
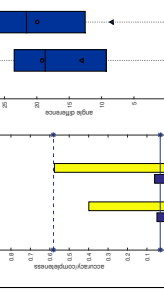
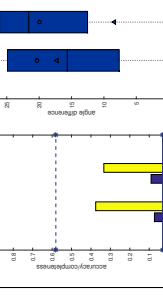
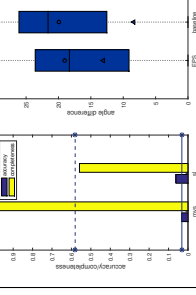
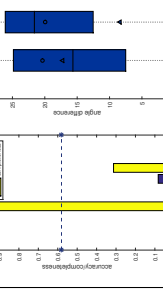
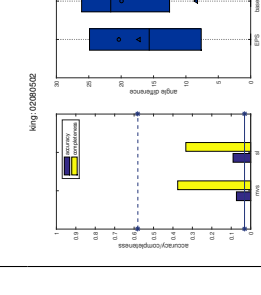
Mapping	Qualitative results				SL
	Quantitative results				
EPS, GSL					
EPS					
PMVS, GSL, EPS					
PMVS, EPS					

Figure 5.18: The first column shows the best algorithm chosen by the mapping. The quantitative and qualitative performance of each technique on the synthetic dataset is also shown. The green dots represent the ground truth while the black dots represent the reconstruction.

way, or a perfect way, since it potentially has the problem of suffering from property scaling issue. Nonetheless, the pairwise analysis remains a valuable approach to obtain insights of the *effective properties* of a specific algorithm. The development of the mapping is an on-going process. For instance, we can include more quantitative metrics such as colour accuracy, ‘ghost reconstruction’, and so on. In order to make the mapping applicable to objects with more complex shapes, we need to consider more sophisticated geometric properties besides roughness, such as concavity, depth-discontinuity, occlusion, etc. Furthermore, the incorporation of more algorithms is another way to ensure that the problem space is well covered.

Chapter 6

An Interpretation of 3D Reconstruction

Now that we have proposed a well-defined problem space of 3D reconstruction problem, as well as a mapping from the problem space to algorithms, the interpretation from the problem-centric description to appropriate algorithms must be shown. There are many possible ways to interpret the description, our proof of concept interpreter is based on the direct evaluation of the performance of each 3D reconstruction algorithm under different problem conditions presented in Chapter 5. This mapping from problem space to algorithms and additional constraints allow an appropriate algorithm to be definitively selected.

The three algorithms and two baseline methods introduced in Chapter 5 have been implemented and integrated into the interpreter, providing basic but well rounded reconstruction capabilities. Although more algorithms can potentially be added, these methods are sufficient to validate the interface's ability to translate descriptions into reconstruction solutions. The integration of new algorithms that are more appropriate under particular situations requires only that they be evaluated by the same process discussed in Chapter 5, as shown in Figure 3.2. This allows researchers to contribute novel algorithms to the interpretation of the interface easily.

Both synthetic and real-world datasets are provided to evaluate the performance of the interpreter. The testbench is made publicly available to encourage the testing of additional reconstruction algorithms. Further, the testbench can be extended to

include new visual/geometric properties, thus providing a wider coverage of the problem space.

This chapter is organized as follows: Section 6.1 provides a roadmap of our evaluation that is centered around one key evaluation question. Section 6.2 proposes a proof-of-concept interpreter. Section 6.4 addresses the evaluation question by demonstrating the robustness of the interpreter using synthetic and real-world datasets, where a satisfactory reconstruction result is returned given the correct description of the object.

6.1 Evaluation Methodology

This thesis proposed a description-based interface to 3D reconstruction problem that hides algorithmic details. The goal of our evaluation is to validate if the proposed interface can translate a user-specified description into an algorithm that gives a successful reconstruction result.

6.1.1 Evaluation question

Can the proof of concept interpreter return an appropriate algorithm that achieves a successful reconstruction given the correct description?

The interface to be evaluated consists of three separate layers, a description, an interpreter, and an algorithm layer. The interpreter is responsible for selecting an appropriate algorithm for reconstruction based on user-specified description. We provide a correct description for each object, and see if the algorithm selected by the interpreter will give an acceptable reconstruction result. The criteria for determining acceptance is detailed below, along with the evaluation steps.

6.1.2 Criteria

Given a correct description of the object, the algorithm chosen by the proof-of-concept interpreter would give a successful reconstruction result. In this thesis, visual inspection is utilized to determine the quality of reconstruction results. More specifically, the result returned by the interface is compared to that of the baseline algorithms to determine if the quality is acceptable. As previously mentioned, the baseline method is chosen so that it always can provide a decent reconstruction

under most circumstances.

The reason that qualitative comparison is sufficient is that we are less interested in developing novel algorithms or improving algorithm performance. If that is the goal, we do need a quantitative comparison among algorithms. However, the goal is to validate if the proposed interface can translate a description into an acceptable result, thus we are more interested in showing that this user-specified description can indeed be interpreted and invoke a good-enough algorithm.

6.1.3 Roadmap

We first need to propose a proof of concept interpreter that is responsible for selecting an appropriate algorithm for reconstruction based on user-specified description. Then we discuss the creation of datasets that are used for evaluation. Finally, we demonstrate the performance of the interpreter by showing the reconstruction results by interpreter-selected algorithm of both synthetic and real-world datasets.

6.2 Interpreter

Our interface consists of three separate layers. The upper layer is the description of the problem condition. The middle layer is the interpreter which receives a description from the user and return an acceptable result. The bottom layer is the actual implementation of the algorithms. The interpreter is responsible for choosing an appropriate 3D reconstruction algorithm based on the description of the problem domain and additional requirements. Thus, it requires an understanding of algorithmic performance across different ranges of problem space to create a suitable interpreter.

However, if the interpreter relies solely on the mapping, it is possible that a user-specified description has more than one corresponding algorithm available. We propose to use two additional constraints so that only one appropriate algorithm is selected.

The first constraint is metric-first or shape-first. There are generally two types of reconstruction results: euclidean/metric reconstruction, and shape reconstruction. The former reconstructs a scene with metric information, but generally gives noisier results. The latter can achieve quality that is only matched by laser scanners

but lack the depth information. The default setting of this constraint is metric-first.

The second constraint is accuracy-first or completeness-first. Methods that achieve high accuracy do not necessarily achieve high completeness. In light of this, the user can choose an algorithm based on the priority level of accuracy and completeness. If multiple algorithm with comparable accuracy or completeness exists, we use a simple ranking system: if one algorithm has the same accuracy but is more complete, or more complete and equally accurate, it is chosen over the others. The default is the accuracy-first constraint.

Thus, the proposed proof of concept interpreter that consists of two components, mapping and constraints, as shown in Figure 6.1. Note that there are many ways of using this mapping information to create an interpreter, and by no means is the proposed one the optimal interpreter.

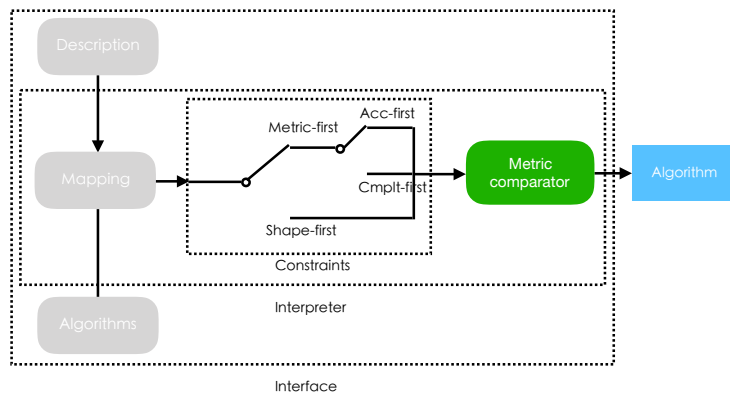


Figure 6.1: Two components of the Interpreter layer. The metric comparator compares the quantitative measures based on the constraints. If ‘acc-first’ is selected, the comparator favours algorithms with lower accuracy value, whereas if ‘cmplt-first’ is selected, the comparator favours algorithms with higher completeness. If ‘shape-first’ is selected, the comparator favours algorithms with lower angular error.

6.3 Overview of Datasets

In this section, we introduce a synthetic and a real-world dataset to evaluate the performance of the interpreter under varied problem conditions. To the best of

our knowledge, there is few publicly available dataset that captures images for algorithms across different categories.

The synthetic dataset contains four objects, as shown in Figure 6.2, and the real-world dataset contains nine objects, four of which are shown in Figure 6.2. Please refer to Figure A.1 for the complete dataset. It covers materials that are representative of four problem conditions proposed in Chapter 3: textureless-diffuse-bright (bust, statue), textureless-mixed-bright (vase0, cup), textured-diffuse-bright (barrel, pot), textured-mixed-bright (vase1, vase). In terms of surface shapes, we have focused mainly on objects with simple geometric properties, namely, smoothly curved surfaces with shallow concavities.

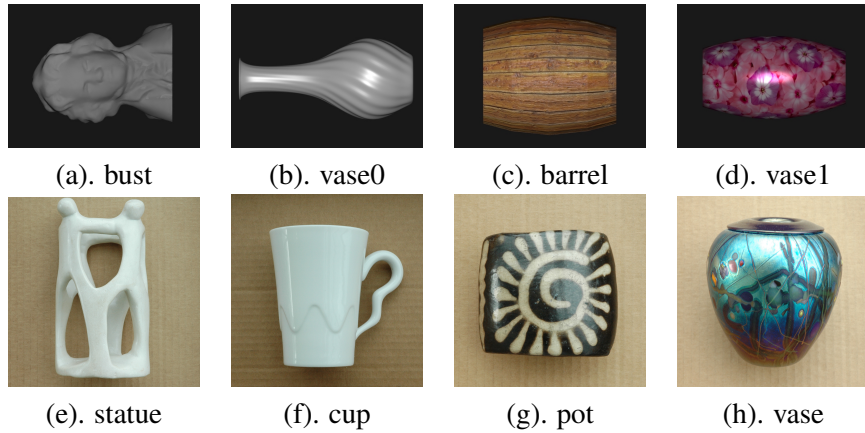


Figure 6.2: (a)-(d): Synthetic dataset, and (e)-(h) real-world dataset for evaluation.

6.3.1 Data capture

The creation of synthetic dataset is largely the same as that discussed in Chapter 5, thus is omitted in this section. The images of real-world dataset are captured using a Nikon D70S camera with a $18 - 70mm$ lens. All images have a resolution of 3004×2000 .

For MVS, we capture the dataset by positioning the camera in three different heights. The objects are about $30 - 50cm$ away from the camera, and stays fixed on a turntable. We have followed the following three steps to acquire data: 1) put

the camera at a different height, adjust the orientation so that the object is at the center of the frame; 2) take pictures while rotating the table. The table rotates approximately 30° every time. We rotate it 12 times and in total, we can obtain 12 images per height.

For PS, a $70 - 200mm$ lens, a handheld lamp, and two reference objects (diffuse and glossy) are used. The objects are positioned about $3m$ from the camera to approximate orthographic projection. To avoid inter-reflection, all data are captured in a dark room with everything covered by black cloth except the target object. We use a hand-held lamp as the light source and choose close to frontal angle to avoid severe self-shadowing effect. We take 20 images per object and select 15 plus images depending on the severity of the self-shadow effect.

For SL, we use a Sanyo Pro xtraX Multiverse projector with a resolution of 1024×768 . The baseline angle is approximately 10° . To avoid the interference of ambient light, and inter-reflection, the objects are captured with room lights off.

6.3.2 Calibration

For MVS, a calibration pattern proposed in [38] is imaged under the object, which is used for calibrating the camera position and orientation by Structure from Motion softwares, such as VisualSfM [65]. The focal length is known a priori and fixed, thus the extrinsic parameters of the camera can be retrieved up to a similarity transformation. Thus, the reconstruction is a metric/euclidean reconstruction.

For PS, though it is preferable to correct the non-linear response of camera, Hertzmann and Seitz discovered that it was unnecessary for EPS. Thus, we did not perform the radiometric calibration step.

For SL, a opensource camera-projector calibration software developed by Moreno and Taubin is used for calibration. This technique works by projecting temporal patterns onto the object, and uses local homography to individually translate each checkerboard corner from the camera plane to the projector plane. This technique can estimate both the intrinsic parameter and camera and projector, and the relative position and orientation.

6.4 Evaluation of Interpreter

This section evaluates the proof of concept interpreter, which should return a successful result given a valid description, or a less successful one given an incorrect description. We choose four different problem conditions where each describes one of the four major classes of objects and provides demonstrative results.

6.4.1 Synthetic Datasets

Each object in the synthetic dataset represents one of the four problem conditions discussed in Section 3. The descriptions of problem conditions of synthetic objects are shown in Table 6.1, as well as the appropriate algorithm selected by the interpreter. Given a user specified description, the proof of concept interpreter will select an algorithm, and any object that matches this description should be well reconstructed by this selected algorithm. Since a description could be mapped to multiple algorithms, an object that does not match the description could potentially have a successful reconstruction result as well. The reconstruction results of synthetic objects and those of the baseline method are shown in Figure 6.3.

Desc#	Object	Texture	Albedo	Spec	Rough	Interp Algo
1	bust	0.2	0.8	0.2	0.8	GSL
2	vase1	0.2	0.8	0.8	0.2	EPS
3	barrel	0.8	0.8	0.2	0.8	GSL
4	vase0	0.8	0.8	0.8	0.2	PMVS

Table 6.1: Problem conditions and interpreted algorithm of the synthetic objects. The description matches the problem condition of corresponding object. The last column shows the algorithm selected by the interpreter.

Desc #	Bust	Vase1	Barrel	Vase0	Interp Algo.
1					GSL
2					EPS
3					GSL
4					PMVS

Figure 6.3: The evaluation of interpreter using synthetic objects. The first column presents the description provided to the interpreter. Description i matches with the problem condition of synthetic object i , which is labeled in green rectangle. The last column is the algorithm selected by the interpreter. Since the interpreter would return a successful reconstruction given a description that matches the problem condition, the quality of reconstruction of the labeled objects indicates success/failure of the interpreter.

Description 1: Bust

Description 2: Vase1

Description 3: Barrel

Description 1 matches with object *barrel*, which has a reliable reconstruction result. The selected algorithm GSL is also in the mapped algorithms of object *bust*, as shown in Table 6.1. Thus even though **description 1** doesn't match with the problem condition of *bust*, a satisfactory result is also returned. However, the selected algorithm is not in the mapped algorithms of object *vase0* and *vase1*, thus less successful results are returned.

Description 4: Vase2

6.4.2 Real-world Datasets

We select four real-world objects, each represents the one of the four problem conditions proposed in Chapter 3, as shown in Figure 6.4. The descriptions of problem conditions of real-world objects are shown in Table A.2, as well as the appropriate algorithm selected by the interpreter. Given a user specified description, the proof of concept interpreter will select an algorithm, and any object that matches this description should be well reconstructed by this selected algorithm. Since a description could be mapped to multiple algorithms, an object that does not match the description could potentially have a successful reconstruction result as well. The reconstruction results of synthetic objects and those of the baseline method are shown in Figure 6.5. Since we do not have the ground truth here, we resort to visual analysis to see if the appropriate algorithm gives an acceptable reconstruction compared to that of the baseline method.

class #	1	2	3	4
description	textureless diffuse bright	textureless mixed d/s bright	textured diffuse dark/bright	textured mixed d/s dark/bright
object				

Figure 6.4: The representatives of the four classes of objects used for evaluation.

We use the aforementioned methods to retrieve the parameters of each property. The decomposition of material for each object is presented in Figure A.1. The property settings of each object is listed in Table A.2.

C#	Object	Texture	Albedo	Specular	Rough	Interp Algo
1	statue	0.2	0.8	0.2	0.8	GSL
2	cup	0.2	0.8	0.5	0.2	EPS
3	pot	0.8	0.8 (0.2)	0.2	0.2	GSL
4	vase	0.8	0.8 (0.2)	0.5	0.2	PMVS

Table 6.2: Problem conditions and interpreted algorithm of the real-world objects. The description matches the problem condition of corresponding object. The last column shows the algorithm selected by the interpreter.

Description 1: statue

Description 2: cup

Description 3: pot

Description 1 matches partially with object *pot* since it has both high and low albedo surface areas. The surface area with high albedo is well reconstructed whereas the surface with low albedo, which doesn't match the description is not reconstructed at all. The selected algorithm is also in the mapped algorithms of object *statue* and *cup*, thus satisfactory results are returned as well. However, this is not the case for object *vase*, thus a very sparse reconstruction is returned.

Description 4: vase

6.5 Sensitivity analysis

[some type of sensitivity analysis is expected here.]

6.6 Summary

Building upon our description and mapping, we are able to develop a proof of concept interpreter which interprets the description of the problem, selects the most appropriate algorithm based on the mapping and returns a reliable reconstruction result. The development of more complex descriptions of object geometry and

Desc #	Statue	Cup	Pot	Vase	Interp Algo.
1					GSL
2					EPS
3					GSL
4					PMVS

Figure 6.5: The evaluation of interpreter using real-world objects. The first column presents the description provided to the interpreter. Description i matches with the problem condition of synthetic object i , which is labeled in green rectangle. The last column is the algorithm selected by the interpreter. Since the interpreter would return a successful reconstruction given a description that matches the problem condition, the quality of reconstruction of the labeled objects indicates success/failure of the interpreter.

material, incorporating new algorithms, and improving mapping are all ongoing processes to improve the interface presented.

Chapter 7

Conclusions

The main contribution of this thesis is the development and application of an interface to 3D reconstruction problem. The significance of this thesis is that not only does it provide a means to reconstruct more general objects, but also does so without requiring knowledge of vision expertise. With the increased sophistication of the vision algorithms, comes the increased barriers to applying these algorithms in real-world applications. Just as personal computer did not become mainstream until the graphical user interface, computer vision algorithm will not become game changing until creative minds from all disciplines can take advantage of these amazing technologies without needing expertise knowledge. To address this challenge, we proposed a three layer interface consisting of description, interpreter, and algorithms.

In the thesis we have presented a taxonomy for 3D reconstruction algorithms based on the conditions surrounding the problem. This object centric taxonomy allows application developers access to advanced vision techniques without requiring sophisticated vision knowledge of the underlying algorithms.

We then discussed a description to 3D reconstruction building upon the proposed taxonomy, which provides an abstraction layer above the underlying vision algorithms. The proposed description provides a formal and definitive way to represent the problem conditions of a 3D reconstruction problem, and based on which, the performance of the algorithm can be evaluated, allowing for a better understanding of the working conditions surround the specific algorithm.

Once we obtained the means to represent problem conditions, we set out to investigate the optimal working conditions surrounding algorithms. This information provides a deeper understanding of performance of algorithms and potentially providing insights into how they may be improved.

Lastly, we demonstrated the usage of the interface by a proof-of-concept interpreter, which returns a successful reconstruction result given a valid description of object's visual and geometric properties.

Extending beyond 3D reconstruction, our proposed general framework of vision is designed to allow all vision tasks more accessible to application developers by providing a description of vision which allows for the description of the problem conditions. In order to provide such accessibility, a representation of the problem space and a means to find the optimal problem space must be well defined. This is a non-trivial task and requires an understanding of the field and an ability to abstract away algorithmic complexity.

7.1 Future directions

3D reconstruction has been one of the most important sub-fields in vision for decades with a range of applications. This thesis focuses on the accessibility of these algorithms instead of developing algorithm novelties. We make several assumptions and simplifications in this thesis, and thus this opens up some potential future directions that can improve the work completed in this thesis.

7.1.1 Geometric Model

The current geometric model fails to capture the complexity of real world objects and focuses mainly on visual properties. Thus, one of the future directions is to develop intuitive geometric models to better describe complex objects.

7.1.2 Property Parameters

We have used a “try-and-see” approach to obtain the property settings of an object, which is based on user judgement and is thus not very rigorous and tends to be tedious. We can use machine learning techniques to obtain visual and geometric information.

7.1.3 Metrics

We have utilized three metrics: accuracy, completeness and angular error. However, there are other measures worth investigating, such as colour accuracy, ‘ghost’ reconstruction error, and so on. Additional metrics such as these can extend the application of our framework, providing more options for developers to choose from.

7.1.4 Mapping Construction

The construction of mapping requires an evaluation of the corresponding algorithm for pairwise properties, which tends not to scale well with respect to the number of properties. Therefore, we need better ways to discover the dependent relation bewteen any two properties.

7.1.5 Interpreter

Currently, implementation of the proof-of-concept interpreter is simplistic and does not fully take advantage of the information we have obtained from the mapping construction process. Therefore, we should develop a more sophisticated interpreter that is more powerful and offers more flexibility.

7.2 Closure

Nowadays, computer vision has been playing a increasing important role in a variety of fields. However, it also takes application developers increasing expertise to apply these technologies to a specific domain. We hope that the efforts in the vision community can be directed to not only develop more advanced algorithms, but to easier access to these algorithms as well.

Bibliography

- [1] Autodesk. URL <http://en.wikipedia.org/wiki/Autodesk>. → pages 1
- [2] Lidar. URL <http://en.wikipedia.org/wiki/Lidar>. → pages 1
- [3] Kinect. URL <http://en.wikipedia.org/wiki/Kinect>. → pages 1
- [4] Vxl c++ libraries for computer vision research and implementation.
<http://vxl.sourceforge.net>. → pages 6
- [5] N. G. Alldrin and D. J. Kriegman. Toward reconstructing surfaces with arbitrary isotropic reflectance: A stratified photometric stereo approach. In *2007 IEEE 11th International Conference on Computer Vision*, pages 1–8. IEEE, 2007. → pages 17
- [6] C. Barnes, E. Shechtman, A. Finkelstein, and D. B. Goldman. PatchMatch: A randomized correspondence algorithm for structural image editing. *ACM Transactions on Graphics (Proc. SIGGRAPH)*, 28(3), Aug. 2009. → pages 9
- [7] S. Barsky and M. Petrou. The 4-source photometric stereo technique for three-dimensional surfaces in the presence of highlights and shadows. *IEEE Transactions on Pattern Analysis and Machine Intelligence*, 25(10):1239–1252, 2003. → pages 16
- [8] S. Berkiten and S. Rusinkiewicz. An RGBN benchmark. Technical report, Technical Report TR-977-16, Princeton University, Feb. 2016. → pages 33
- [9] F. Bernardini, H. Rushmeier, I. M. Martin, J. Mittleman, and G. Taubin. Building a digital model of michelangelo’s florentine pieta. *IEEE Computer Graphics and Applications*, 22(1):59–67, 2002. → pages 1
- [10] F. Blais. Review of 20 years of range sensor development. *Journal of Electronic Imaging*, 13(1), 2004. → pages 8

- [11] R. C. Bolles and P. Horaud. 3dpo: A three-dimensional part orientation system. *The International Journal of Robotics Research*, 5(3):3–26, 1986. → pages 27
- [12] G. Bradski and A. Kaehler. *Learning OpenCV: Computer vision with the OpenCV library.* ” O'Reilly Media, Inc.”, 2008. → pages 6
- [13] E. N. Coleman and R. Jain. Obtaining 3-dimensional shape of textured and specular surfaces using four-source photometry. *Computer graphics and image processing*, 18(4):309–328, 1982. → pages 16
- [14] C. H. Esteban and F. Schmitt. Silhouette and stereo fusion for 3d object modeling. *Computer Vision and Image Understanding*, 96(3):367–392, 2004. → pages 9
- [15] O. Faugeras and R. Keriven. *Variational principles, surface evolution, pde's, level set methods and the stereo problem.* IEEE, 2002. → pages 1, 9
- [16] R. W. Fleming. Visual perception of materials and their properties. *Vision research*, 94:62–75, 2014. → pages 32, 33
- [17] R. W. Fleming, R. O. Dror, and E. H. Adelson. Real-world illumination and the perception of surface reflectance properties. *Journal of vision*, 3(5):3–3, 2003. → pages 33
- [18] R. W. Fleming, C. Wiebel, and K. Gegenfurtner. Perceptual qualities and material classes. *Journal of vision*, 13(8):9–9, 2013. → pages 32
- [19] S. Fuhrmann, F. Langguth, and M. Goesele. Mve-a multiview reconstruction environment. In *Proceedings of the Eurographics Workshop on Graphics and Cultural Heritage (GCH)*, volume 6, page 8, 2014. → pages 7
- [20] Y. Furukawa and J. Ponce. Accurate, dense, and robust multiview stereopsis. *IEEE transactions on pattern analysis and machine intelligence*, 32(8):1362–1376, 2010. → pages 1, 7, 9, 38
- [21] S. Galliani, K. Lasinger, and K. Schindler. Massively parallel multiview stereopsis by surface normal diffusion. In *Proceedings of the IEEE International Conference on Computer Vision*, pages 873–881, 2015. → pages 9, 10
- [22] M. Goesele, B. Curless, and S. M. Seitz. Multi-view stereo revisited. In *2006 IEEE Computer Society Conference on Computer Vision and Pattern Recognition (CVPR'06)*, volume 2, pages 2402–2409. IEEE, 2006. → pages 1, 10

- [23] D. B. Goldman, B. Curless, A. Hertzmann, and S. M. Seitz. Shape and spatially-varying brdfs from photometric stereo. *IEEE Transactions on Pattern Analysis and Machine Intelligence*, 32(6):1060–1071, 2010. → pages 17
- [24] H. Hayakawa. Photometric stereo under a light source with arbitrary motion. *JOSA A*, 11(11):3079–3089, 1994. → pages 16
- [25] J. Heller, M. Havlena, M. Jancosek, A. Torii, and T. Pajdla. 3d reconstruction from photographs by cmp sfm web service. In *Machine Vision Applications (MVA), 2015 14th IAPR International Conference on*, pages 30–34, May 2015. doi:10.1109/MVA.2015.7153126. → pages 7
- [26] A. Hertzmann and S. M. Seitz. Example-based photometric stereo: Shape reconstruction with general, varying brdfs. *IEEE Transactions on Pattern Analysis and Machine Intelligence*, 27(8):1254–1264, 2005. → pages 16, 38, 69
- [27] V. H. Hiep, R. Keriven, P. Labatut, and J.-P. Pons. Towards high-resolution large-scale multi-view stereo. In *Computer Vision and Pattern Recognition, 2009. CVPR 2009. IEEE Conference on*, pages 1430–1437. IEEE, 2009. → pages 9
- [28] B. K. Horn. Shape from shading: A method for obtaining the shape of a smooth opaque object from one view. 1970. → pages 13
- [29] I. Ihrke, K. N. Kutulakos, H. Lensch, M. Magnor, and W. Heidrich. Transparent and specular object reconstruction. In *Computer Graphics Forum*, volume 29, pages 2400–2426. Wiley Online Library, 2010. → pages 23
- [30] H. Jin, S. Soatto, and A. J. Yezzi. Multi-view stereo beyond lambert. In *Computer Vision and Pattern Recognition, 2003. Proceedings. 2003 IEEE Computer Society Conference on*, volume 1, pages I–I. IEEE, 2003. → pages 11
- [31] H. Jin, S. Soatto, and A. J. Yezzi. Multi-view stereo reconstruction of dense shape and complex appearance. *International Journal of Computer Vision*, 63(3):175–189, 2005. → pages 11
- [32] M. Kazhdan, M. Bolitho, and H. Hoppe. Poisson surface reconstruction. In *Proceedings of the fourth Eurographics symposium on Geometry processing*, volume 7, 2006. → pages 7

- [33] P. D. Kovesi. MATLAB and Octave functions for computer vision and image processing. Available from: <<http://www.peterkovesi.com/matlabfn/>>. → pages 6
- [34] K. N. Kutulakos and S. M. Seitz. A theory of shape by space carving. *International Journal of Computer Vision*, 38(3):199–218, 2000. → pages 1, 9
- [35] M. Levoy, K. Pulli, B. Curless, S. Rusinkiewicz, D. Koller, L. Pereira, M. Ginzton, S. Anderson, J. Davis, J. Ginsberg, et al. The digital michelangelo project: 3d scanning of large statues. In *Proceedings of the 27th annual conference on Computer graphics and interactive techniques*, pages 131–144. ACM Press/Addison-Wesley Publishing Co., 2000. → pages 1
- [36] M. Lhuillier and L. Quan. Match propagation for image-based modeling and rendering. *IEEE Transactions on Pattern Analysis and Machine Intelligence*, 24(8):1140–1146, 2002. → pages 9
- [37] M. Lhuillier and L. Quan. A quasi-dense approach to surface reconstruction from uncalibrated images. *IEEE transactions on pattern analysis and machine intelligence*, 27(3):418–433, 2005. → pages 9
- [38] B. Li, L. Heng, K. Koser, and M. Pollefeys. A multiple-camera system calibration toolbox using a feature descriptor-based calibration pattern. In *Intelligent Robots and Systems (IROS), 2013 IEEE/RSJ International Conference on*, pages 1301–1307. IEEE, 2013. → pages 69
- [39] S. P. Mallick, T. E. Zickler, D. J. Kriegman, and P. N. Belhumeur. Beyond lambert: Reconstructing specular surfaces using color. In *2005 IEEE Computer Society Conference on Computer Vision and Pattern Recognition (CVPR’05)*, volume 2, pages 619–626. Ieee, 2005. → pages 16
- [40] G. Mariottini and D. Prattichizzo. Egt: a toolbox for multiple view geometry and visual servoing. *IEEE Robotics and Automation Magazine*, 3(12), December 2005. → pages 6
- [41] D. Marr. Vision: A computational investigation into the human representation and processing of visual information. 1982. → pages 9
- [42] D. Moreno and G. Taubin. Simple, accurate, and robust projector-camera calibration. In *3D Imaging, Modeling, Processing, Visualization and Transmission (3DIMPVT), 2012 Second International Conference on*, pages 464–471. IEEE, 2012. → pages 69

- [43] P. Moulon, P. Monasse, R. Marlet, and Others. Openmvg. an open multiple view geometry library. <https://github.com/openMVG/openMVG>. → pages 7
- [44] S. K. Nayar, K. Ikeuchi, and T. Kanade. Surface reflection: physical and geometrical perspectives. Technical report, DTIC Document, 1989. → pages 30
- [45] S. Nishida and M. Shinya. Use of image-based information in judgments of surface-reflectance properties. *JOSA A*, 15(12):2951–2965, 1998. → pages 33
- [46] G. P. Otto and T. K. Chau. region-growing algorithm for matching of terrain images. *Image and vision computing*, 7(2):83–94, 1989. → pages 9
- [47] T. Poggio, V. Torre, and C. Koch. Computational vision and regularization theory. *Nature*, 317(6035):314–319, 1985. → pages 7
- [48] C. Rocchini, P. Cignoni, F. Ganovelli, C. Montani, P. Pingi, and R. Scopigno. Marching intersections: an efficient resampling algorithm for surface management. In *Shape Modeling and Applications, SMI 2001 International Conference on.*, pages 296–305. IEEE, 2001. → pages 18
- [49] S. Roy and I. J. Cox. A maximum-flow formulation of the n-camera stereo correspondence problem. In *Computer Vision, 1998. Sixth International Conference on*, pages 492–499. IEEE, 1998. → pages 8
- [50] J. Salvi, J. Pages, and J. Batlle. Pattern codification strategies in structured light systems. *Pattern recognition*, 37(4):827–849, 2004. → pages 11
- [51] Y. Sato and K. Ikeuchi. Temporal-color space analysis of reflection. *JOSA A*, 11(11):2990–3002, 1994. → pages 16
- [52] K. Schluns. Photometric stereo for non-lambertian surfaces using color information. In *International Conference on Computer Analysis of Images and Patterns*, pages 444–451. Springer, 1993. → pages 16
- [53] S. M. Seitz and C. R. Dyer. Photorealistic scene reconstruction by voxel coloring. In *Computer Vision and Pattern Recognition, 1997. Proceedings., 1997 IEEE Computer Society Conference on*, pages 1067–1073. IEEE, 1997. → pages 8
- [54] S. M. Seitz, B. Curless, J. Diebel, D. Scharstein, and R. Szeliski. A comparison and evaluation of multi-view stereo reconstruction algorithms. In *2006 IEEE Computer Society Conference on Computer Vision and*

- Pattern Recognition (CVPR'06)*, volume 1, pages 519–528. IEEE, 2006. → pages 1, 8, 10, 36, 38
- [55] L. Sharan, R. Rosenholtz, and E. Adelson. Material perception: What can you see in a brief glance? *Journal of Vision*, 9(8):784–784, 2009. → pages 32
 - [56] B. Shi, Z. Wu, Z. Mo, D. Duan, S.-K. Yeung, and P. Tan. A benchmark dataset and evaluation for non-lambertian and uncalibrated photometric stereo. In *Proceedings of the IEEE Conference on Computer Vision and Pattern Recognition*, pages 3707–3716, 2016. → pages 36
 - [57] W. M. Silver. *Determining shape and reflectance using multiple images*. PhD thesis, Massachusetts Institute of Technology, 1980. → pages 16
 - [58] N. Snavely, S. M. Seitz, and R. Szeliski. Photo tourism: exploring photo collections in 3d. In *ACM transactions on graphics (TOG)*, volume 25, pages 835–846. ACM, 2006. → pages 7
 - [59] Y. Uh, Y. Matsushita, and H. Byun. Efficient multiview stereo by random-search and propagation. In *3D Vision (3DV), 2014 2nd International Conference on*, volume 1, pages 393–400. IEEE, 2014. → pages 9
 - [60] A. Vedaldi and B. Fulkerson. VLFeat: An open and portable library of computer vision algorithms. <http://www.vlfeat.org/>, 2008. → pages 6
 - [61] G. Vogiatzis, P. H. Torr, and R. Cipolla. Multi-view stereo via volumetric graph-cuts. In *Computer Vision and Pattern Recognition, 2005. CVPR 2005. IEEE Computer Society Conference on*, volume 2, pages 391–398. IEEE, 2005. → pages 8
 - [62] G. Vogiatzis, C. H. Esteban, P. H. Torr, and R. Cipolla. Multiview stereo via volumetric graph-cuts and occlusion robust photo-consistency. *IEEE Transactions on Pattern Analysis and Machine Intelligence*, 29(12):2241–2246, 2007. → pages 8, 10
 - [63] R. J. Woodham. Photometric stereo: A reflectance map technique for determining surface orientation from image intensity. In *22nd Annual Technical Symposium*, pages 136–143. International Society for Optics and Photonics, 1979. → pages 13
 - [64] R. J. Woodham. Photometric method for determining surface orientation from multiple images. *Optical engineering*, 19(1):191139–191139, 1980. → pages 1, 14, 17

- [65] C. Wu et al. Visualsfm: A visual structure from motion system. 2011. → pages 7, 69
- [66] R. Zhang, P.-S. Tsai, J. E. Cryer, and M. Shah. Shape-from-shading: a survey. *IEEE transactions on pattern analysis and machine intelligence*, 21(8):690–706, 1999. → pages 14
- [67] E. Zheng, E. Dunn, V. Jovic, and J.-M. Frahm. Patchmatch based joint view selection and depthmap estimation. In *Proceedings of the IEEE Conference on Computer Vision and Pattern Recognition*, pages 1510–1517, 2014. → pages 9
- [68] T. E. Zickler, P. N. Belhumeur, and D. J. Kriegman. Helmholtz stereopsis: Exploiting reciprocity for surface reconstruction. *International Journal of Computer Vision*, 49(2-3):215–227, 2002. → pages 17

Appendix A

Supporting Materials

A.1 Definition of 3D Reconstruction

We will first provide definitions of some basic concepts, which include general computer vision concepts such as scene, camera, and image. We then define a few other terms that are closely related to the reconstruction problem. We then provide reasonable approximations for a more practical definition of the problem as a whole.

A.1.1 Basic notations

We will use the following notations: $\{C_n\}_{n=0}^{N-1}$ represents the camera set, which includes both intrinsic and extrinsic parameters; $\{I_n\}_{n=0}^{N-1}$ represents the set of all images; $\{L_n\}_{n=0}^{N-1}$ represents the set of light sources.

Definition 1 (Scene) The scene S is the four-dimensional joint spatio-temporal target of interest.

Definition 2 (Image) The image refers to the 2D observation of the 3D scene S on the image plane of camera C_i at time t_0 , which is modelled as: $I_i = T(S, C_i, L_0, t_0)$, or on the image plane of C_0 under the light source L_i at time t_i , $I_i = T(S, C_0, L_i, t_i)$, where T is the geometric/radiometric transformation.

T can be a geometric transformation which determines the 2D coordinates of a 3D point, or a radiometric transformation which determines the intensity/irradiance information from the information of illumination, viewing direction and surface

orientation.

A.1.2 Segment and Scell

Definition 3 (Segment) A segment (seg) is a distinct region in the image, and is the most basic element in the image, which can be considered as a generalized pixel.

For instance, a segment can be a pixel, a window area, an edge, a contour, or a region of arbitrary size and shape.

Definition 4 (Cue) Cues are the visual or geometric characteristics of the segments seg that can be used for reconstruction, denoted as $cue(seg)$.

For instance, the cue can be the texture within a window area, the intensity-/colour value of a pixel, or the object contour, etc.

Definition 5 (Scell) A scell (scene element, denoted as sc) is a volume in the scene which corresponds to at least one segment. A scell can be considered as a generalization of a voxel.

Definition 6 (Property) Properties are the visual and geometric characteristics of the scell sc , which would influence the cues of a segment, denoted as $prop(sc)$.

The property of the scell can be the 3D position or orientation information, visual texture, reflectance, surface orientation, roughness, convexity, etc.

The relation between the terms defined above is shown in Figure A.1.

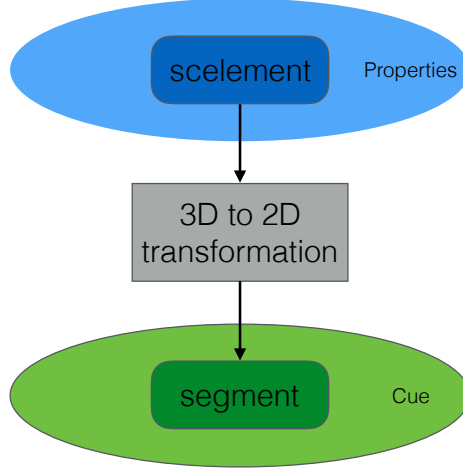


Figure A.1: Relation between a scell and a segment

A.1.3 Consistency

Every photograph of a 3D scene taken from a camera C_i partitions the set of all possible scenes into two families, those that reproduce the photograph and those that do not. We characterize this constraint for a given shape and a given radiance assignment by the notion of *consistency*.

Definition 7 (Consistency criterion) The consistency criterion checks whether the properties of a scell sc can produce the cues observed in the corresponding segment seg .

$$\begin{aligned} \text{consist}(\text{prop}(sc), \text{cue}(seg)) = 1 &\Rightarrow \text{consistent} \\ \text{consist}(\text{prop}(sc), \text{cue}(seg)) = 0 &\Rightarrow \text{not consistent} \end{aligned}$$

Definition 8 (Segment consistency) Let S be the scene. A scell $s \in S$ that is visible from C_i is consistent with the image I_i if and only if the consistency criterion is true.

Definition 9 (Image consistency) A scene S is image consistent with image I_i if any scell $\forall s \in S$ visible from the camera C_i is segment consistent with this image.

Definition 10 (Scene consistency) A scene S is scene consistent with a set of images $\{I_n\}_{n=0}^{N-1}$ if it's image consistency with each image $I_i \in \{I_n\}_{n=0}^{N-1}$ in the set.

A.1.4 Formal Definition

Definition 11 (3D reconstruction problem) Given a set of images $\{I_n\}_{n=0}^{N-1}$ captured by cameras $\{C_n\}_{n=0}^{N-1}$, or under a set of light sources $\{L_n\}_{n=0}^{N-1}$, find a set of scells $\{sc_m\}_{m=0}^{M-1}$ such that any scell is consistent with the visible images in the set $\{I_n\}_{n=0}^{N-1}$, i.e., $\forall sc_i \in \{sc_m\}_{m=0}^{M-1}$, we have the following:

$$\text{consist}(\text{prop}(sc_i), \text{cue}(seg_{(i,j)})) = 1.$$

where $seg_{(i,j)}$ is the corresponding segment of sc_i in camera C_j . Alternatively, 3D reconstruction tries to find a set of scells $\{sc_m\}_{m=0}^{M-1}$ that are scene consistent with the image set $\{I_n\}_{n=0}^{N-1}$

A.1.5 Applied Definition

While the definition presented above gives a formal definition of the problem of 3D reconstruction, it is not necessarily applicable in a practical setting. In this section, we extend this formal definition to an approximate, yet applied version.

Definition 12 (Consistency score) The consistency score measures the similarity between a scell sc and the corresponding segment seg .

$$\begin{aligned} \text{consist}(\text{prop}(sc), \text{cue}(seg)) &= x, x \in [0, 1] \\ \text{consist}(\text{prop}(sc), \text{cue}(seg)) = 1 &\Rightarrow \text{consistent} \\ \text{consist}(\text{prop}(sc), \text{cue}(seg)) = 0 &\Rightarrow \text{not consistent} \end{aligned}$$

Definition 13 (Applied consistency criterion) A scell sc and a segment seg are considered consistent if the the consistency score is above a pre-defined threshold ε .

$$\text{consist}(\text{prop}(sc), \text{cue}(seg)) > \varepsilon$$

Definition 14 (Applied 3D Reconstruction Problem) Given a set of images $\{I_n\}_{n=0}^{N-1}$ captured by cameras $\{C_n\}_{n=0}^{N-1}$, or under a set of light sources $\{L_n\}_{n=0}^{N-1}$, find a set of scells $\{sc_m\}_{m=0}^{M-1}$ such that the consistency score between the set of scells and their corresponding segments $\{seg_{(i,j)}\}_{i=0, j=0}^{M-1, N-1}$ are maximized.

$$\text{maximize} \quad \sum_{j=0}^{N-1} \sum_{i=0}^{M-1} \text{consist}(\text{prop}(sc_i), \text{cue}(seg_{(i,j)}))$$

A.2 Definition of Radiometric Terms

Below is a list of radiometry terms, see Figure A.2 for an illustration:

- Solid angle ($d\omega$): 3D counterpart of angle, $d\omega = \frac{dA \cos \theta_i}{R^2}$ (steradian).
- Projected solid angle ($d\Omega$): $d\Omega = \cos \theta d\omega$.
- Incident radiance ($\mathbf{L}_i(\theta_i, \phi_i)$): light flux received from the direction (θ_i, ϕ_i) on a unit surface area, unit ($\text{watt} \cdot \text{m}^{-2} \cdot \text{steradian}^{-1}$).

- Irradiance ($E_i(\theta_i, \phi_i)$): light Flux (power) incident per unit surface area from all direction, $E_i(\theta_i, \phi_i) = \int_{\Omega_i} L_i(\theta_i, \phi_i) d\Omega_i$ (watt/m²).
- Surface radiance ($L_r(\theta_r, \phi_r)$): light flux emmited from a unit surface area in the direction (θ_r, ϕ_r) , unit (watt · m⁻² · steradian⁻¹).

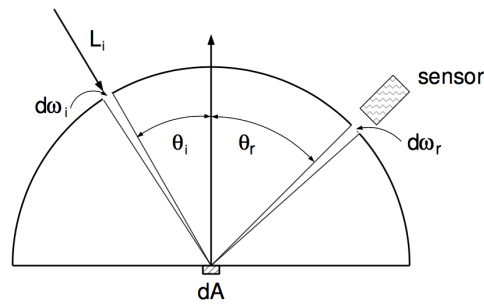


Figure A.2: Illustration of light-matter interaction.

A.3 Material of real-world objects

A.4 Parameters of real-world objects

A.5 Results of real-world objects



(a). box



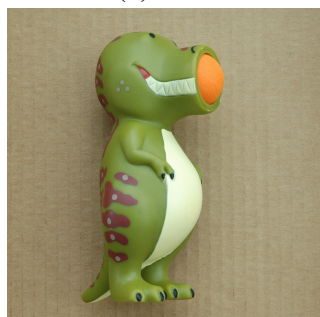
(b). cat0



(c). cat1



(d). cup



(e). dino



(f). house



(g). pot



(h). statue



(i). vase

Table A.1: Images of the real-world objects.

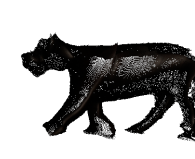
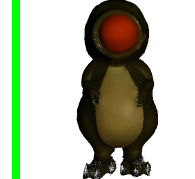
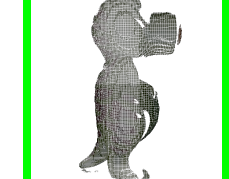
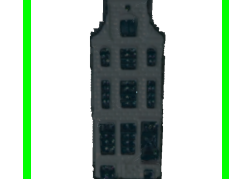
Mapping	PMVS	EPS	GSL	VH (BL)
PMVS, EPS, GSL				
PMVS				
None				
EPS, GSL				
EPS, GSL				
PMVS, GSL				

Figure A.3: Reconstruction results of MVS, PS, SL, and the baseline method VH.

Class	Texture	Albedo	Specularity	Roughness	Mapping
box	0.8	0.8	0.2	0.8	PMVS, EPS, GSL
cat0	0.5	0.5	0.2	0.2	PMVS
cat1	0.2	0.2	0.2	0.2	None
cup	0.2	0.8	0.5	0.2	EPS, GSL
dino	0.2	0.5,	0.2	0.8	EPS, GSL
		0.8			
house	0.8	0.2,	0.2	0.2	PMVS, GSL
		0.8			
pot	0.8	0.2,	0.2	0.2	PMVS
		0.5			
status	0.2	0.8	0.2	0.8	EPS, GSL
vase	0.8	0.2,	0.5	0.2	PMVS
		0.5			

Table A.2: Property list for the real-world objects

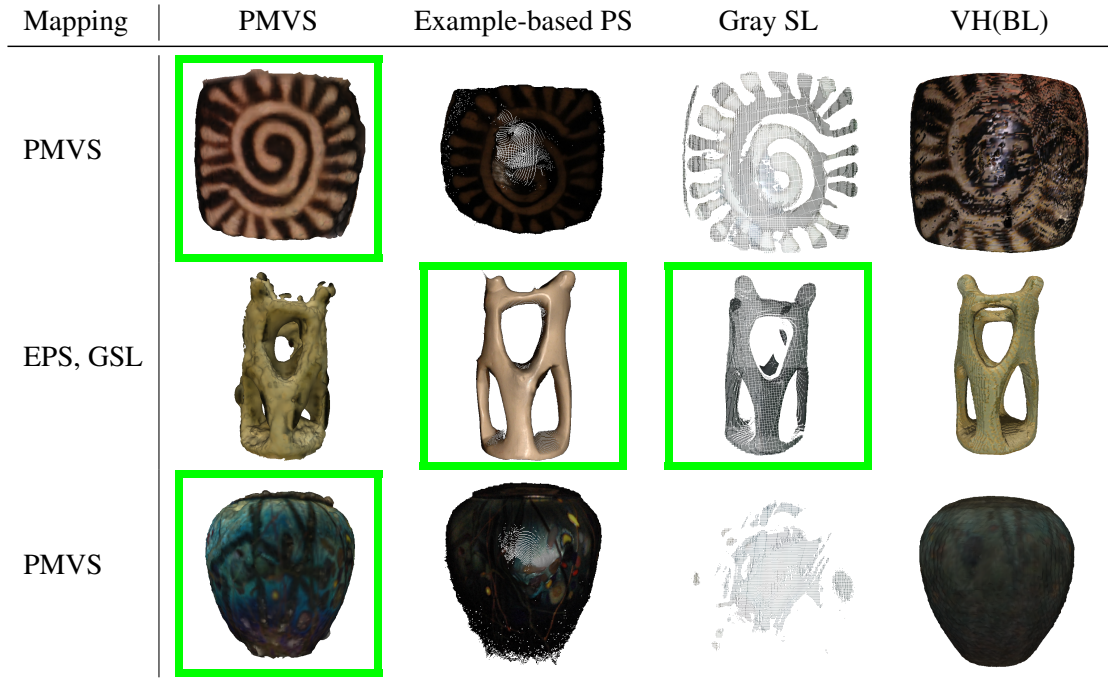


Figure A.4: Reconstruction results of MVS, PS, SL, and the baseline method VH (cont'd).